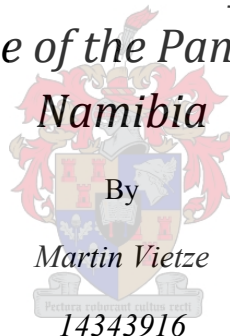




UNIVERSITEIT
STELLENBOSCH
UNIVERSITY

*Geology and emplacement controls of the Stinkbank granite in
the south Central Zone of the Pan-African Damara Belt,
Namibia*



By

Martin Vietze

14343916

Thesis presented in partial fulfillment of the requirements for the degree of

Master of Science

At the University of Stellenbosch

2009

Supervised by Prof. Alex Kisters and Prof. Gary Stevens

5. THE STINKBANK GRANITE AND RELATED PHASES

The Stinkbank granite forms part a prominent and compositionally diverse group of granites regionally referred to as Salem-type granites (*Jacob, 1974*). Although compositionally heterogeneous, Salem-type granites show a number of unifying features. The granites all tend to intrude at a similar stratigraphic level within the Damara Supergroup, namely above the Karibib Formation and within the Kuiseb Formation (*Jacob, 1974; Miller, 1983, 2008*). The granites also commonly intrude into the hinge zones of regional-scale synforms within the central Damara Belt (*Smith 1965; Miller, 2008*). The heterogeneous nature of the granites is displayed by mineralogical variations and the presence of compositionally distinct phases. These variations are explained by either (1) in-situ fractionation processes at the emplacement site, (2) variable degrees of wall-rock assimilation of particular metaturbiditic wall rocks of the Kuiseb Formation through the granites, or (3) multiple intrusive relationships (*summarized by Miller, 2008*). The latter forms a very important part in this study of the emplacement controls of the Stinkbank granite, since compositionally distinct phases of the granite seem to define an intrusion sequence. As with other Salem-type granites, three main granite varieties can be distinguished in the Stinkbank granite, henceforth referred to as 1) *leucogranite*, 2) *leucocratic megacrystic Stinkbank granite*, and 3) *biotite-rich, megacrystic Stinkbank granite*. The distribution of the granite phases is shown in Figure 5.1

5.1 Field appearance and distribution of granite varieties within the Stinkbank granite

5.1.1 Leucogranite

Leucogranites are by far the most abundant of the three granite varieties. Dominating the SW parts of the Stinkbank granite (Figure 5.1), they form large, whaleback-like platforms and prominent pavements that can reach up to 50-70 m in height above the erosional plain of the Khan River. Large platforms of leucogranite also outcrop in the NE around coordinates 1) 22° 7'43.31"S; 15°24'53.92"E, 2) 22° 8'25.81"S; 15°24'40.51"E, 3) 22° 6'26.16"S; 15°27'0.33"E and outcrops indicate that the leucogranite is continuous along the SW contact between the Stinkbank granite and the wall-rocks of the Kuiseb Formation. Where contacts are exposed, the leucogranite is in sharp and direct contact with the Kuiseb Formation.

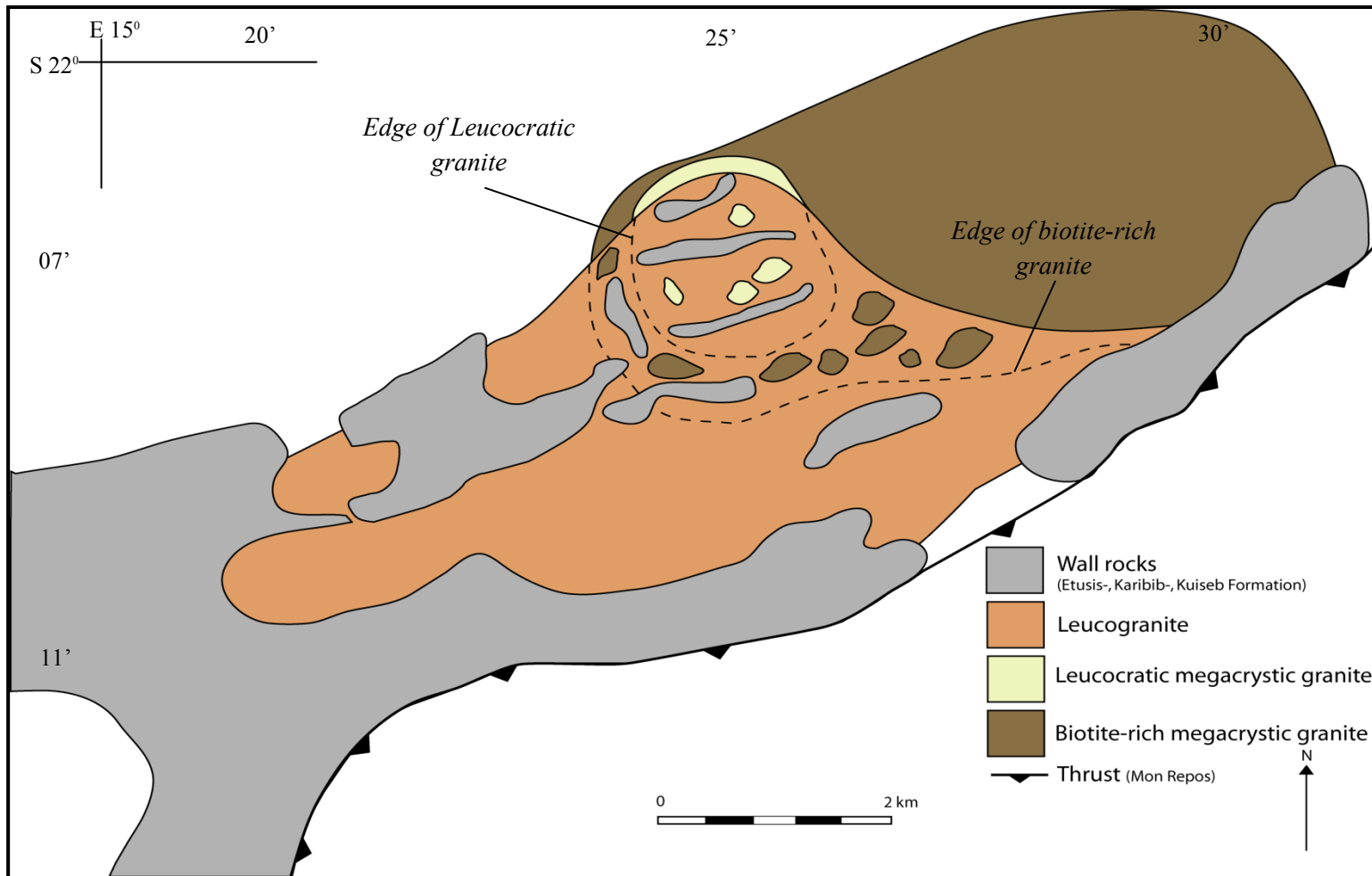


Figure 5.1, Simplified spatial distribution of the main granite phases in the Stinkbank granite.

The leucogranite has a fine- to medium-grained texture and consists of quartz, plagioclase, perthite K-feldspar, biotite, muscovite, tourmaline, garnet (Figure 5.2, a, b), zircon and monazite. In general, leucogranites of the Stinkbank granite show igneous textures containing subeuhedral K-feldspar and plagioclase. Plagioclase contains characteristic growth twinning and is commonly fresh, whereas K-feldspar tends to show sericitization. In places, both plagioclase and K-feldspar show marginal recrystallization into smaller grain aggregates. Quartz shows signs of recrystallization, including subgrain formation and grain-boundary migration, resulting in lobate grain boundaries, as well as undulose extinction, but it may also have relatively straight grain boundaries. Biotite is strongly pleochroic, reddish brown and generally only a few millimetres in length (Figure 5.2, c). Tourmaline makes up approx 1-2 % of the bulk mineralogy of the rock. It is easily spotted in thin section under plain polarized light being developed as green, euhedral and prismatic minerals with characteristic trigonal sections normal to the crystallographic c-axis (Figure 5.2, d). The invariably fresh tourmaline is commonly zoned, showing a bluish core, surrounded by an olive green rim. Zircon is a common accessory, occurring as large, mm-sized euhedral and zoned crystals as well as small inclusions in biotite, where they are surrounded by characteristic heterokinetic halos. Monazite has been reported as a common accessory of the Stinkbank granite by Marlow (1983), but could not be identified in this study.

For the most part, the leucogranite contains a NE-SW trending solid-state fabric. The fabric is defined by the preferred alignment of biotite as well as, in places, quartz ribbons and ovoid, marginally recrystallized quartz-feldspar aggregates. A magmatic fabric is, in places, indicated by schlieren textures, expressed by undulating and anastomosing, up to several meter long wispy aggregates of biotite. The rock is very light in colour and weathers to a light yellow/creamy colour (Figure 5.2, e). The leucogranites are compositionally and texturally very homogeneous over large areas and internal contacts or sheets are only rarely observed. The leucogranite contains inclusions of wall-rock strata (mainly banded schists and metapsammities of the Kuiseb Formation), and older granite phases.

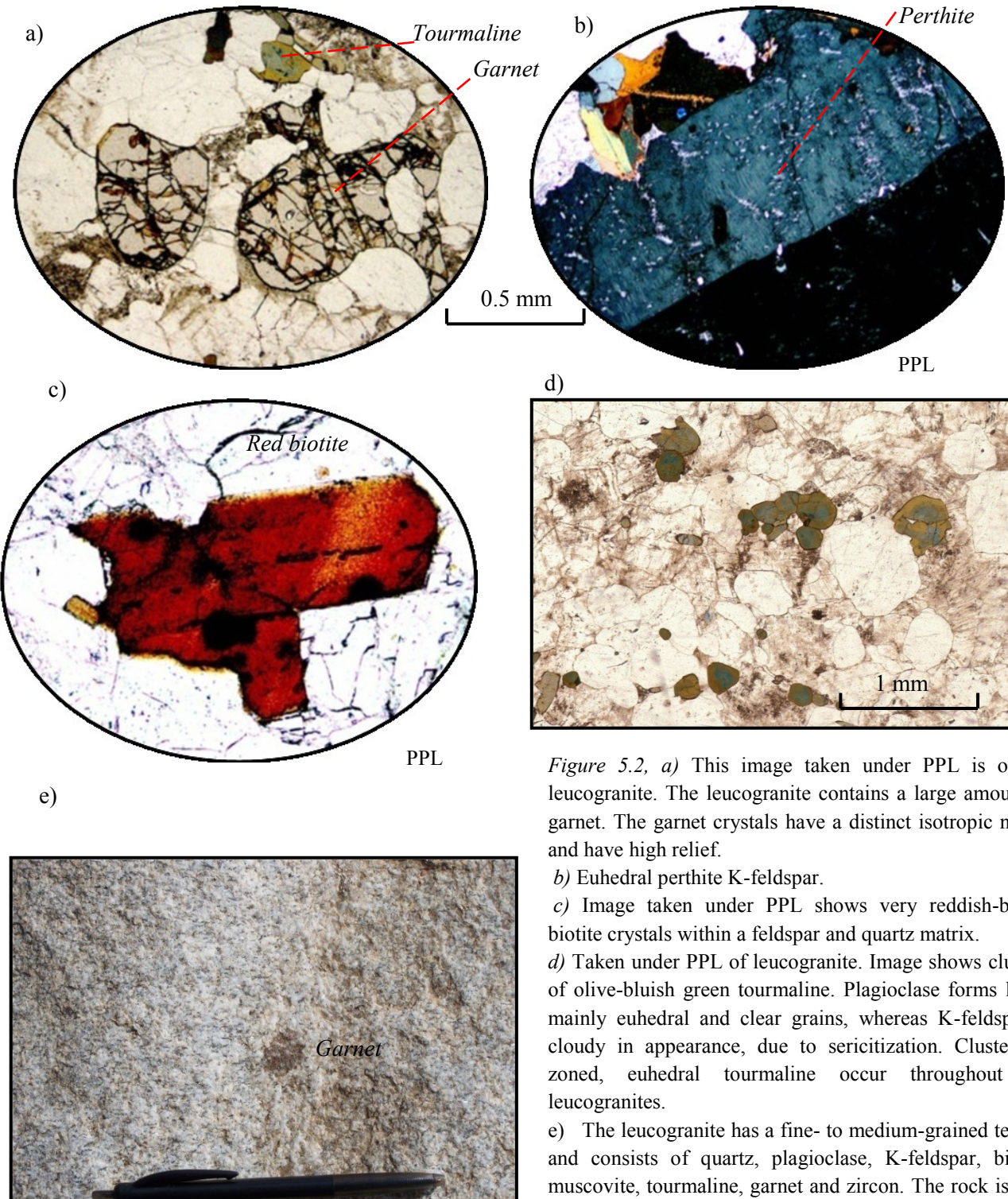


Figure 5.2, a) This image taken under PPL is of the leucogranite. The leucogranite contains a large amount of garnet. The garnet crystals have a distinct isotropic nature and have high relief.

b) Euhedral perthite K-feldspar.

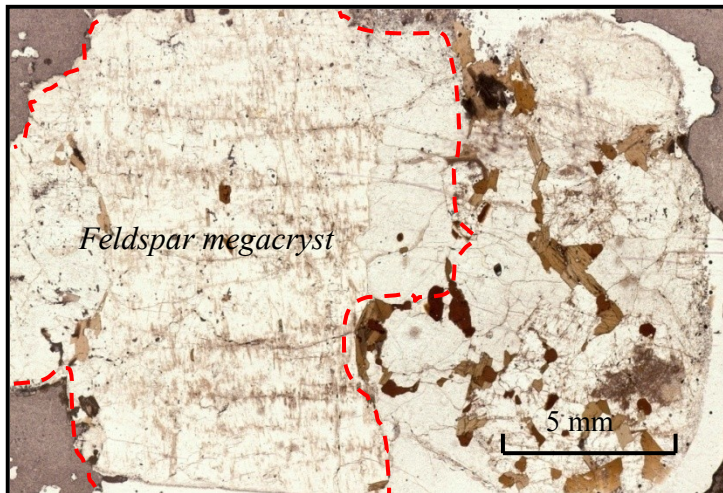
c) Image taken under PPL shows very reddish-brown biotite crystals within a feldspar and quartz matrix.

d) Taken under PPL of leucogranite. Image shows clusters of olive-bluish green tourmaline. Plagioclase forms large, mainly euhedral and clear grains, whereas K-feldspar is cloudy in appearance, due to sericitization. Clusters of zoned, euhedral tourmaline occur throughout the leucogranites.

e) The leucogranite has a fine- to medium-grained texture and consists of quartz, plagioclase, K-feldspar, biotite, muscovite, tourmaline, garnet and zircon. The rock is very light in colour and weathers to a light yellow/ creamy colour

5.1.2 Leucocratic megacrystic Stinkbank granite

Leucocratic, megacrystic granites form a distinct, but volumetrically subordinate granite phase within the Stinkbank granite. These granites are mostly exposed in the central-SW portion of the Stinkbank granite and Kransberg syncline, around the Pramberg ($22^{\circ} 7'55.99''\text{S}$, $15^{\circ}24'54.77''\text{E}$, Appendix 1). The granite consists of large (up to 4 cm long) megacrystic K-feldspar, plagioclase, quartz and biotite (Figure 5.3, a). Biotite is strongly pleochroic, reddish-brown in colour and generally only 1-3 millimetres in length. Compared to the leucogranite, no tourmaline could be identified in the megacrystic leucogranite. Quartz shows weak undulose extinction, indicating recrystallization. As with the leucogranite, the feldspars are sub-euhedral and the plagioclase displays characteristic twinning under cross-polarized light. Locally, the granite contains a fabric that is defined by the alignment of the large, white K-feldspar phenocrysts (Figure 5.3, b). Good outcrops of the leucocratic megacrystic Stinkbank granite can be found at localities: 1) $22^{\circ} 7'55.94''\text{S}$; $15^{\circ}24'54.30''\text{E}$, 2) $22^{\circ} 7'55.35''\text{S}$; $15^{\circ}24'20.44''\text{E}$ 3) $22^{\circ} 8'17.69''\text{S}$; $15^{\circ}23'52.84''\text{E}$ (Appendix 1)



a)

Figure 5.3, a) Image taken with PPL of leucocratic megacrystic granite. The image shows a large, partly sericitized (cloudiness) K-feldspar megacryst, set in a finer grained matrix of quartz, plagioclase, K-feldspar, biotite (brown) and opaques. The preferred orientation of biotite imparts a weak foliation on the rock.



b)

Figure 5.3, b) Plan view of the leucocratic, megacrystic Stinkbank granite. The photo shows large, aligned feldspar megacrysts in a quartz-feldspar-biotite matrix.

5.1.3 Biotite-rich, megacrystic Stinkbank granite

The biotite-rich megacrystic granite (Figure 5.4, a) is very distinct and the second most abundant granite in the Stinkbank granite. It is mostly exposed in the central portion of the Kransberg syncline and in the NE parts of the study area, occupying aerially extensive, relatively flat platforms and gently undulating ridges around the Khan River. In these northern parts of the Stinkbank granite, it is the biotite-rich megacrystic granite that is commonly in close contact with the wall rocks of the Kuiseb Formation. In outcrop, it is a dark-grey, medium- to coarse-grained, commonly well-foliated granite, containing quartz (20-30%), plagioclase (15-30%), brownish-red biotite (20-30%) (Figure 5.4, b) and K-feldspar (15-30%) (Figure 5.4, c and d) with accessory subeuhedral and zoned zircon, sericite, allanite, garnet and opaques. K-feldspar megacrysts can be up to 4 cm's in length (Figure 5.4, e). The microcline phenocrysts occur as optically zoned, tabular crystals containing randomly oriented biotite and plagioclase inclusions. The abundance of K-feldspar megacrysts varies, and they may occur as both isolated crystals in individual outcrops as well as closely spaced (5-10 cm) clusters. Quartz, plagioclase and K-feldspar in the matrix occur as equant to irregularly-shaped grains 0.5 to 1 mm in diameter. Both plagioclase and microcline are often altered to fine-grained, white mica. Biotite within the matrix is light- to dark-brown, strongly pleochroic reaching, on average, 0.5 mm in length.

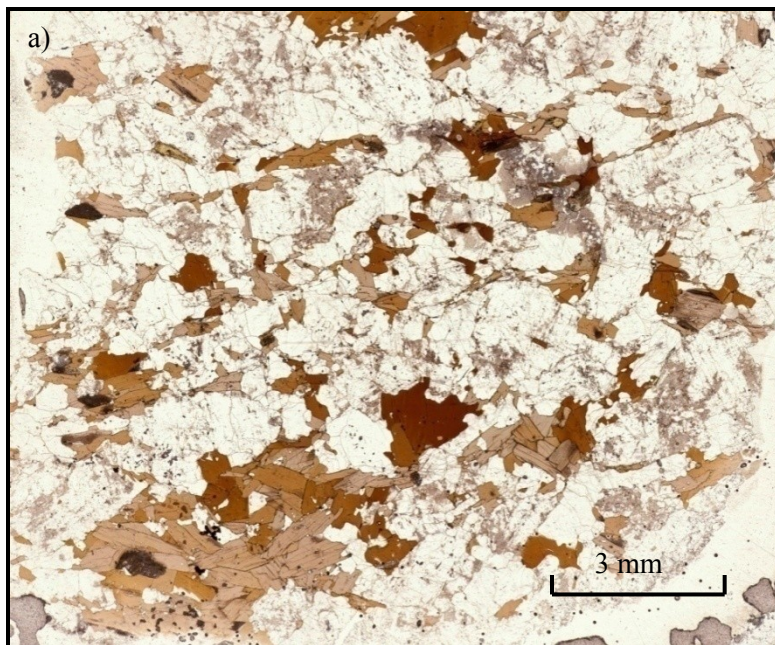
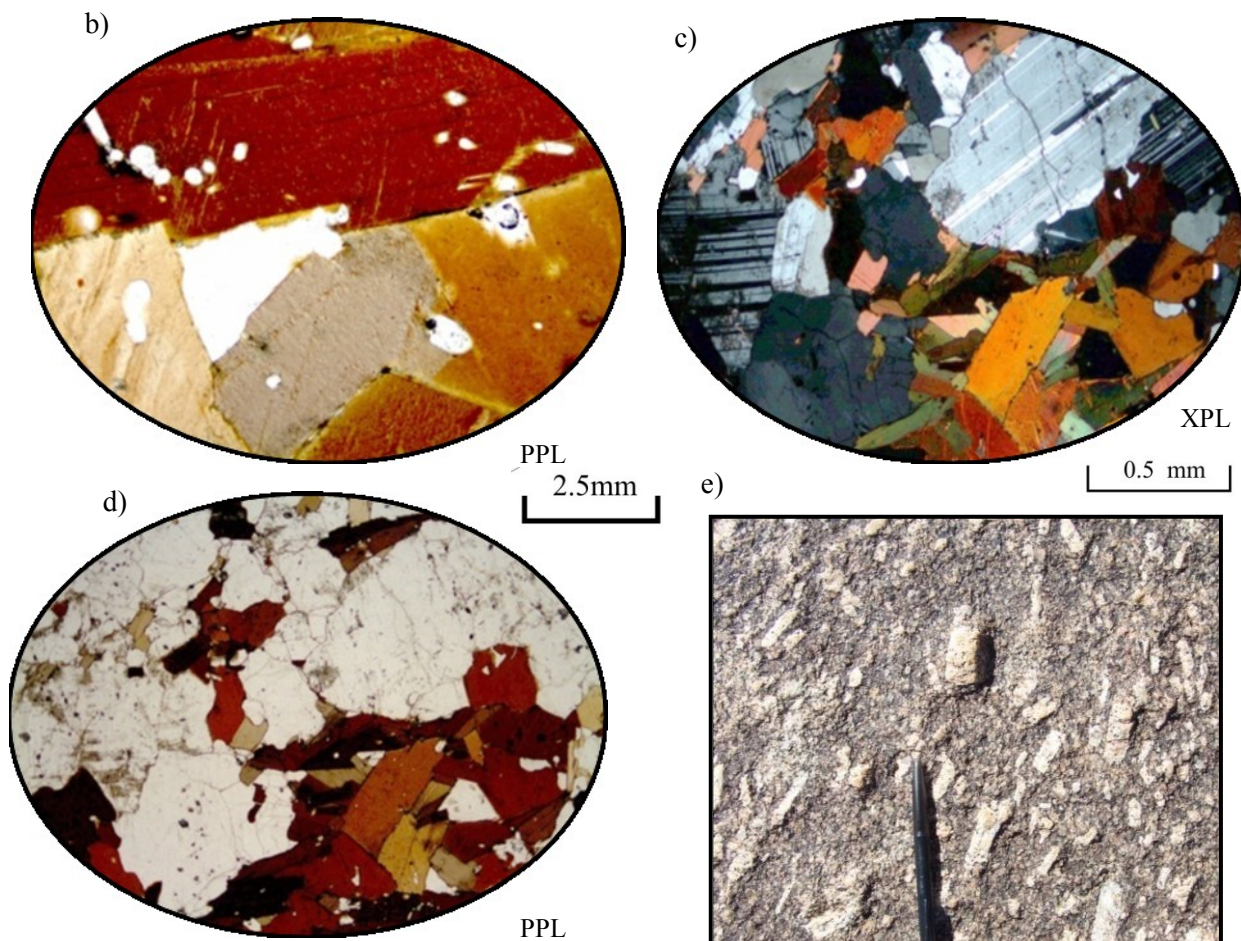


Figure 5.4, a) Image taken with PPL of biotite-rich megacrystic Salem-type granite. The image shows a large amount of reddish brown biotite amongst a medium-grained quartz-feldspar matrix. Biotite commonly shows a preferred alignment to produce a fabric within this granite.



b) (PPL) Brown-red biotite. The biotite in the biotite-rich Stinkbank granite is much browner than the biotite in the leucogranite.

c) Image taken using XPL to illustrate the distinct lamellar twinning within plagioclase and igneous textures.

d) Same image as taken in *c)*, but under PPL. It shows the biotite minerals within the quartz and K-feldspar matrix.

e) Plan view of the biotite-rich megacrystic Stinkbank granite, showing aligned K-feldspar megacrysts in a finer-grained, biotite-rich matrix

5.1.4 Sill- and dyke-like intrusions

Coarse-grained granites with often pegmatitic textures are ubiquitous in the field area. Based primarily on their geometry, two main types are distinguished, namely (1) bedding- and/or foliation-parallel sheets or sills (Figure 5.5), and (2) cross-cutting dykes, that intrude the wall rocks and the main phases of the Stinkbank granite at various angles.



Figure 5.5, Cross-sectional view of the southern limb of the Kransberg syncline. Picture was taken in an E direction. A large amount of granitic sills intrude the Kuiseb schist wall-rocks, and make up approx. 10 - 20 % of the overall volume of the wall-rocks. The contact between the wall-rocks and the Stinkbank granite is 30 m to the left of the image.

Sills are most common in wall-rocks of the Kuiseb Formation. They show steep- to vertical attitudes in domain 1, on the SW limb of the Kransberg Syncline, and rotate with the bedding and the S_1 foliation in domain 2 of the SW termination of Kransberg Syncline and the Stinkbank granite. Compositionally, the sills closely resemble the leucogranite phase of the Stinkbank granite, consisting of quartz, K-feldspar, plagioclase, biotite and muscovite, tourmaline and garnet. However, grain sizes are much coarser and textures are commonly pegmatitic with K-feldspar crystals reaching up to 20 cm in diameter, or tourmaline needles up to 5 cm in length (Figure 5.6 and 5.7). In addition, tourmaline and muscovite can make up to 15 vol. % of individual sills, which contrasts with the composition of the main leucogranite. Depending on the abundance of K-feldspar, tourmaline and muscovite, colours vary between bright white and deep red-pinkish, so that sills are easy to identify within dark-brown schists of the Kuiseb Formation. Sheet-like intrusions in the wall rocks that would resemble the biotite-rich, megacrystic Stinkbank granite are conspicuous by their absence.

The sills vary in thickness from merely cm-wide stringers to massive bodies exceeding 10-15 m in width. Most common widths are 10-50 cm. Large sills show evidence of multiple intrusive relationships, indicated by textural and mineralogical variations and cross-cutting relationships between different intrusions (Figure 5.6). Tourmaline typically forms comb structures perpendicular to the sill walls and also outlines multiple intrusive relationships within sills, documenting the sheeted and, thus, composite nature of many sills (Figure 5.6). Numerous sills display an internal zonation of feldspar- and tourmaline-rich margins and quartz-feldspar-muscovite-rich cores (Figure 5.7). In places, the amalgamation of several sills leads to the formation of small pegmatite stocks, some 50-100 m in strikelength and up to 30-50 wide in particularly antiformal fold (F_2) hinges (Chapter 5.3).

Dykes show sharply cross-cutting relationships with the transposed bedding of the wall rocks. The dykes may show similar compositions and textures compared to the pegmatitic sills, but fine- and even-grained granite dykes are more common than in sills. Steeply-dipping dykes are rare, whereas shallowly-dipping dykes that cross-cut bedding and sills at high-angles are more common (Figure 5.8). Cross-cutting dykes also occur in the interior of the Stinkbank granite. These parallel sided dykes are commonly between 10-100cm wide and can be traced for hundreds of meters along strike, outcrop permitting.

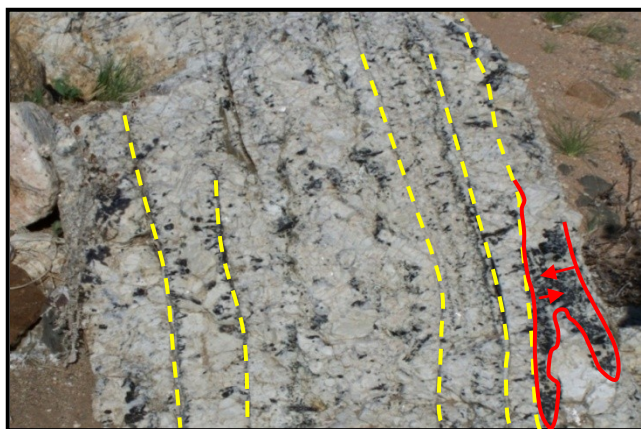


Figure 5.6, Oblique view of a leucocratic pegmatite, situated within the southern limb of the Kransberg syncline. The pegmatite is ca. 1.2 m wide and shows an internal layering or sheet-like structure. Individual sheets are outlined by the comb-like, inward growth of tourmaline crystals (black) and the difference in grainsizes.



Figure 5.7, This pegmatitic sill displays an internal zonation of feldspar- and tourmaline-rich margins and quartz-feldspar-muscovite-rich cores.

A third, distinct geometry of pegmatites is found in the central portions of the Kransberg syncline, commonly situated along the contacts between rocks of the Kuiseb Formation and Salem- type granites, particularly the biotite-rich megacrystic Stinkbank granite. These pegmatites form irregularly-shaped, rather lensoid pods, not exceeding lengths of 10 meters. The contacts are irregular and the pegmatite usually crosscuts the older lithologies.

As mentioned in Chapter 4.5.1, sills and dykes in the wall rocks of the Stinkbank granite display variable degrees of deformation. The common chocolate-tablet boudinage of sills and upright symmetrical folding of shallowly dipping dykes are both consistent with the bulk NW-SE shortening strain during D₂. A further important observation is that deformed and undeformed dykes and/or sills may occur in the same outcrops (Figures 5.8 and 5.9), pointing to the relative timing of sheet intrusion and a protracted period of sheet emplacement. Moreover, earlier and abundant granite sheeting in the wall rock can be seen to influence the emplacement of later granite sheets.

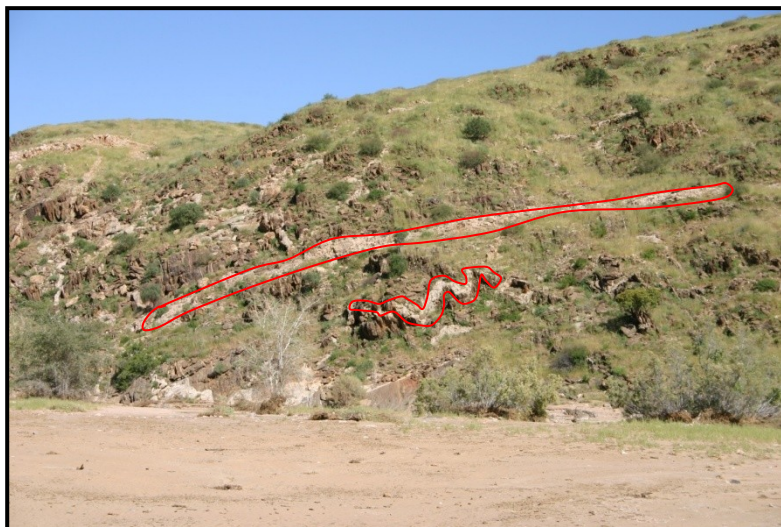


Figure 5.8, Cross-sectional view through a section of the S-limb of the Kransberg syncline. Shallowly-dipping pegmatite dykes (annotated by red line) crosscut the steeply-dipping bedding of the Kuiseb Formation. Note that the lower dyke has been folded into near-upright, NE-trending F₂ folds, whereas the top dyke is rather post-tectonic. Khan River, looking SW.

This relative timing and overprinting relationship of different granite sheet geometries is well displayed in outcrops of domain 1, along the southern flank of the Kransberg synform (e.g. at coordinates 22° 8'23.56"S; 15°28'36.69"E (Appendix 1) (Figure 5.9 and 5.10). The earliest generation of sheets intruded as steep bedding-parallel sills. Repeated subvertical granite sheeting is indicated by sheet-in-sheet intrusive contacts. The amalgamation of granite and

pegmatite sills leads to the formation of a more or less massive, 80-100 m wide granite outcrop (Figure 5.9 and 5.10). This granite is cross-cut by a set of shallow SE dipping granite sheets. Individual granite and pegmatite sheets are clearly distinguished by variations in grain size and composition, as well as cross-cutting contacts. These granite sheets are folded into upright open-to close folds (Figure 5.9 and 5.10). The folded granites, in turn, are cross-cut by subhorizontal, planar and undeformed, 2-3 m thick pegmatite sheets (Figure 5.10, bottom)

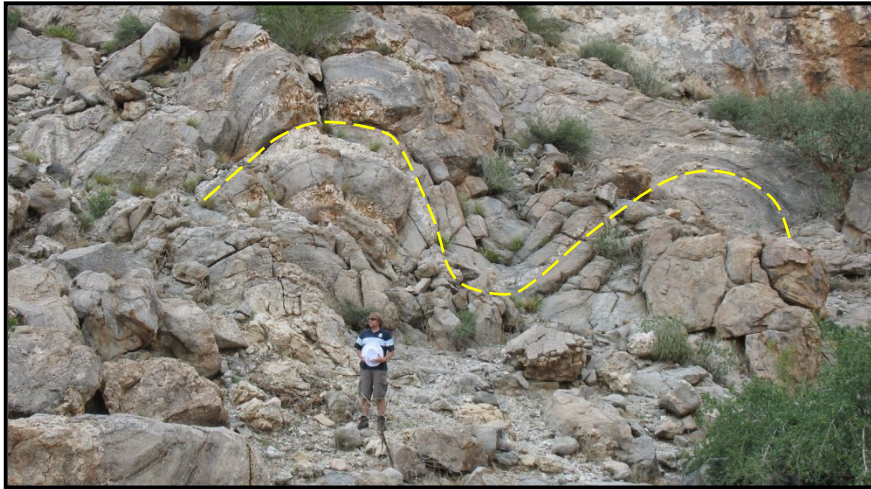


Figure 5.9, Small scale granite pluton comprising of multiple granite sheets which have all intruded in different orientations (vertical and horizontal). The area shown here contains initially horizontal folded granite sheets (indicated by the dashed red line).

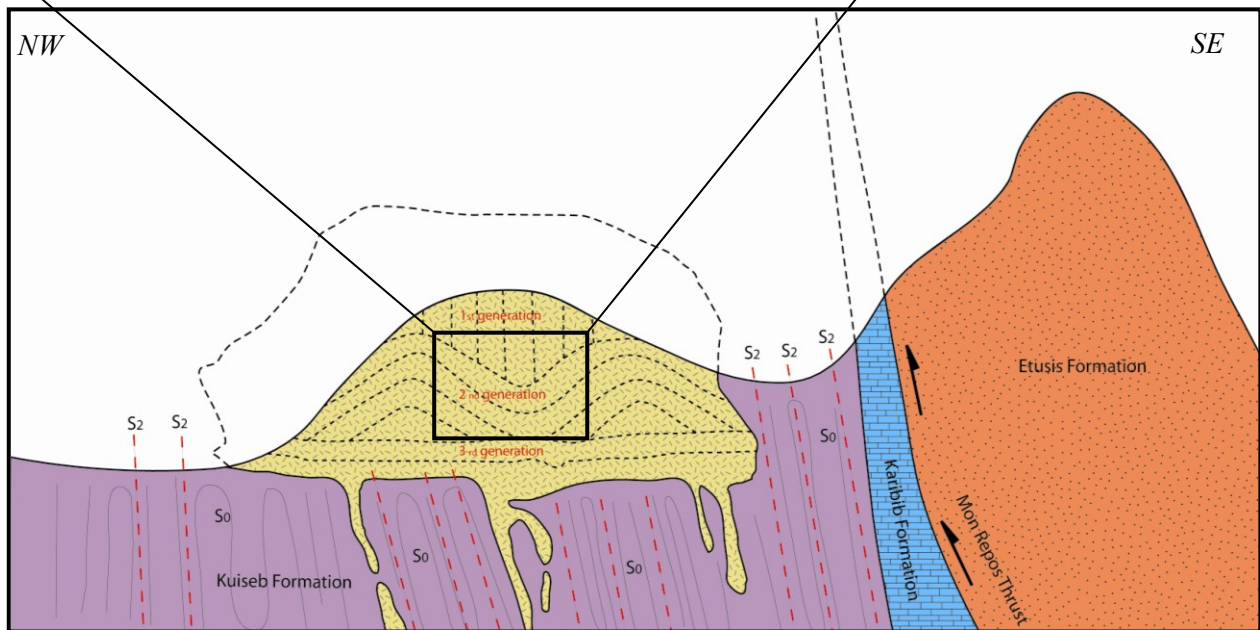


Figure 5.10, Schematic cross section through the SW limb of the Kransberg syncline. The central granite pluton represents the amalgamation of three distinct, sheet-like granite geometries. Cross-cutting relationships indicate an early generation of steeply-dipping, closely spaced sills, cross-cut by a second generation of subhorizontal granite sheets, now folded, that are, in turn, cross-cut by a last generation of subhorizontal, undeformed pegmatite sheets.

5.2 Fabric development in the Stinkbank granite

For the most part, all three granite phases of the Stinkbank granite contain magmatic and solid-state fabrics, although fabric intensities vary (a) with rock type, and (b) spatially within individual granite phases.

The distinction and differentiation of fabrics in the Stinkbank granite follows the criteria devised by, *inter alia*, Paterson et al. (1989), Vernon (2000, 2004), Miller and Paterson (1994) and McLaren and Pryer (2001) for the description and origin of fabrics in granites. Magmatic and solid-state fabrics in granites represent two end-members of a potentially gradual fabric development that essentially tracks different amount of melts during the progressive crystallization of granite plutons (Paterson et al., 1989). Magmatic flow and resulting magmatic fabrics involve a change of shape of the magma in the presence of a melt phase. With a sufficient amount of melt in the crystallizing granite pluton, crystals may rotate passively into alignment without internal deformation. The structural and microstructural evidence for magmatic flow includes the preferred alignment of elongate euhedral magmatic crystals; the imbrication or tiling of magmatic phases; the elongation of microgranitoid enclaves without plastic deformation of the minerals; magmatic flow foliations and elongate microgranitoid enclaves deflected around xenoliths and phenocrysts; or schlieren of crystals, mostly mafic minerals formed by sorting during magmatic flow, with no plastic deformation of minerals involved. Solid state fabrics are formed when a high ratio of crystals to melt during progressive crystallization of magmas inhibits the free rotation and alignment of crystals in the melt phase. Instead, deformation is accommodated by mainly solid-state deformation mechanisms of magmatic phases. Ductile deformation and crystal-plastic deformation mechanisms dominate at higher temperatures following the initial crystallization and cooling of the plutons. Grain-boundary migration and the recrystallization of grains, associated reduction in the size of grains, the development of recrystallized tails, especially on feldspar phenocrysts and/or boudinage of strong minerals can be expected during high-temperature solid-state deformation (*e.g.* Vernon 2004). If deformation continues during the cooling of the pluton, brittle processes such as cataclasis of initially feldspar and, at lower temperatures, quartz may characterize low-temperature solid-state deformation,

recrystallization and internal deformation of grains. Core-and-mantle microstructures are very typical for solid state deformation.

The biotite-rich megacrystic granite contains a magmatic as well as solid-state foliation. The fabrics are very widespread, found throughout the entirety of the granite outcrop, although fabric intensities vary. The magmatic fabric is defined primarily by the preferred orientation of K-feldspar megacrysts (Figure 5.11).



Figure 5.11, biotite-rich megacrystic Stinkbank granite with a magmatic fabric defined by the orientation of K-feldspar megacrysts. The magmatic fabric trends approximately NE-SW.

Over large areas, the megacrysts are euhedral without signs of marginal recrystallization (Figure 5.11), indicating their alignment in the presence of a melt phase. Although the alignment of K-feldspar megacrysts is almost ubiquitous within biotite-rich megacrystic granite, the whaleback-type outcrops in the low-lying central NE parts only yielded a few three-dimensional readings of the magmatic foliation. Hence, only the trend of the foliation as defined by the long axes of the megacrysts in given, defining a very pronounced NE trend, parallel to the S_2 fabric in wall rocks and the general structural grain of the Damara Belt. A solid-state fabric in the granite is parallel to the magmatic fabric. The solid-state fabric is expressed by the preferred alignment of biotite aggregates (Figure 5.12) and flattened, disc-shaped quartz grains. Moreover, the locally observed marginal recrystallization of feldspar megacrysts may result in augen-like structures and near gneissic textures in highly-strained areas. Highly-strained varieties of the biotite-rich granite can also be mistaken, for example, with schists of the Kuiseb Formation, but isolated K-feldspar megacrysts are a good indicator of the granitic precursor. Schlieren textures are shown in Figure 5.13.



Figure 5.12, alignment of biotite aggregates within the leucogranite. Representing the solid state fabric S_2 . The solid state fabric trends approximately NE-SW.



Figure 5.13, biotite aggregates, or schlieren within the leucogranite. Representing the magmatic fabric S_2 . The magmatic fabric trends approximately NE-SW.

The megacrystic leucogranite shows a very similar fabric development. The euhedral megacrysts commonly define a well-developed NE trending magmatic fabric (Figure 5.14). Solid state fabrics are defined by the preferred orientation of biotite and flattened quartz-discs. The marginal recrystallization of feldspar megacrysts is less common compared to the biotite-rich megacrystic granite.



Figure 5.14, euhedral K- feldspar megacrysts within the leucocratic megacrystic Stinkbank granite, define a well- developed NE trending magmatic fabric.

Regionally developed magmatic fabrics are more difficult to identify in the medium- and even-grained leucogranite. On large pavements in the SW central parts of the granite, schlieren textures are defined by wispy biotite aggregates that can be traced for several meters along strike. These are interpreted to define a magmatic foliation. The trend of the schlieren is NE. A solid-state foliation is more widespread, although fabric intensities vary. Leucogranites adjacent to domain 1, parallel to the steep SW limb of the Kransberg syncline show a well developed NE trending solid-state foliation by the preferred orientation of fine-grained biotite and quartz discs. The latter may form quartz ribbons with, in places, aspect ratios of > 5 to 1. This fabric is also present in leucogranites in the SW termination of the Stinkbank granite, but fabric intensities are significantly lower here. Due to the mainly whaleback-like outcrops, no linear fabrics could be observed on the foliation planes.

In summary, the Stinkbank granite is characterized by the presence of both magmatic and solid-state foliations. The foliations show a general NE trend, parallel to the S_2 fabric of the wall rocks and the regional structural grain of the Damara Belt (Figure 5.15). Fabric intensities seem to show systematic variations, being generally stronger in the biotite-rich megacrystic granite and weaker, though present, in the leucogranite. Fabric intensities also show a spatial variability, being stronger adjacent to domain 1, parallel to the limb of the Kransberg syncline. Fabric intensities are low adjacent to domain 2, in the SW hinge of the syncline and the termination of the Stinkbank granite.

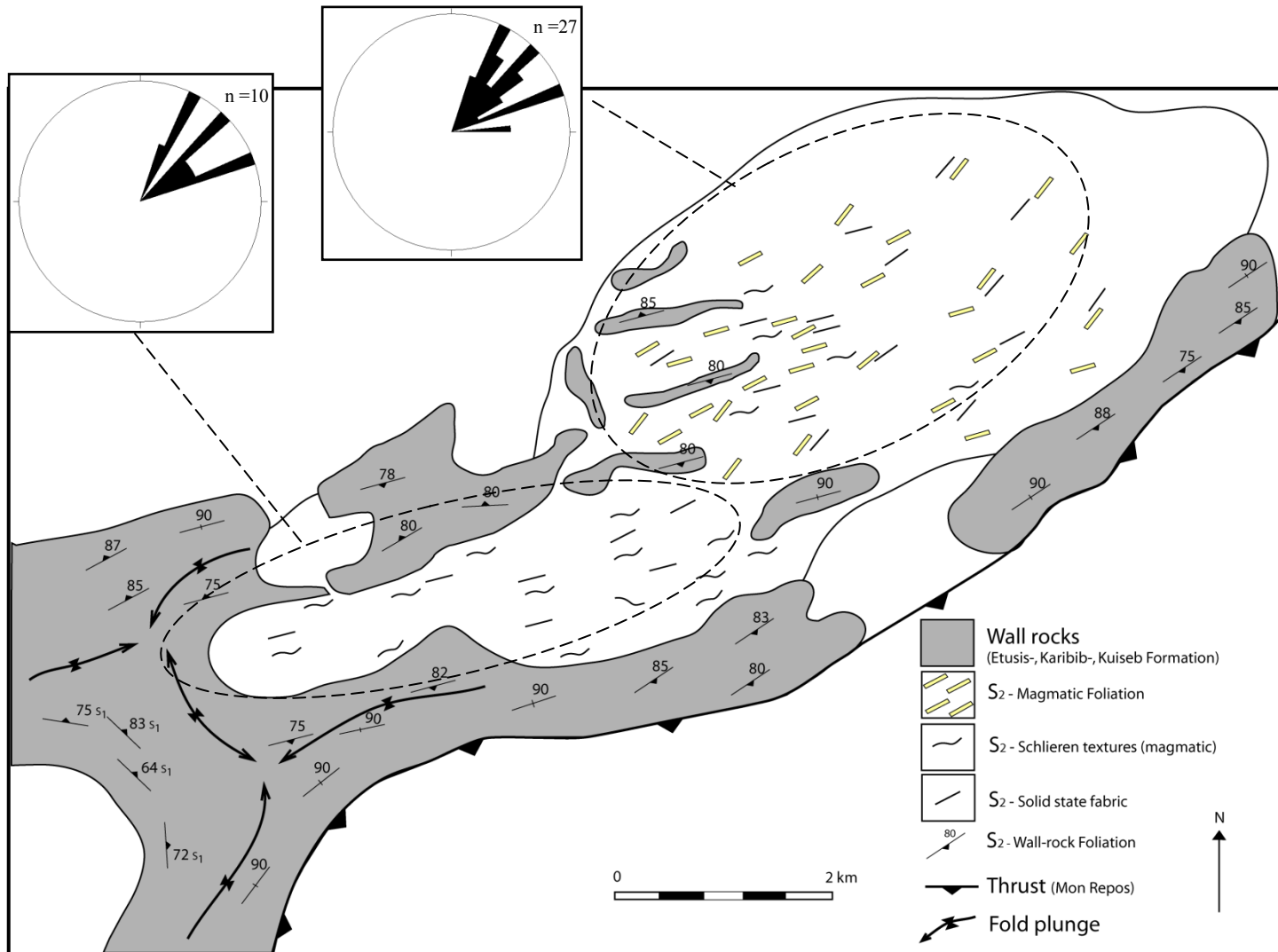


Figure 5.15, Structural Map, illustrating S₂-magmatic foliation, solid state foliation and S₂-wall-rock foliation in the Stinkbank Granite. The two stereonets display the NE-SW fabric trend that exists within the three phases of the Stinkbank granite. This fabric is defined by the preferred orientation of the biotite-, large K-spar minerals and schlieren. Fabrics are all vertical, thus the straight lines in the stereonets. Stresses are inferred as the strains are of a coaxial nature (Chapter 4.5.1).

5.3 Internal architecture of the Stinkbank granite

5.3.1 Intrusive and relative age relationships

Intrusive relationships provide an indication of the relative timing of different granite phases. The biotite-rich, megacrystic Stinkbank granite is the first of the main granite phases. It is clearly intruded by both the leucogranite and megacrystic leucogranite that contain xenoliths of the biotite-rich megacrystic granite (Figure 5.16).



Figure 5.16, Oblique view of a whaleback leucogranite outcrop. Xenoliths of the darker, biotite-rich megacrystic granite are floating within the leucogranite. This clearly indicates the timing relationship between the two granites

Moreover, platforms underlain by the biotite-rich granite in the NE parts of the Stinkbank granite are commonly intruded by either meter-wide dykes and apophyses of leucogranite or larger, irregularly shaped pods of leucogranite. The biotite-rich megacrystic Stinkbank granite, in turn, only contains wall-rock xenoliths of the Kuiseb Formation. Johnson (2005) described enclaves of more mafic igneous rocks in the biotite-rich granite, some 10 km to the N of the study area, but these were not observed in the present study area. The leucogranite, in turn, contains xenoliths of the megacrystic leucogranite. This indicates an intrusive relationship from earlier biotite-rich megacrystic granite, via leucocratic megacrystic granite to late-stage leucogranite for the main phases of the Stinkbank granite. This relative age relationship corresponds well with sequence of intrusions described for other Salem-type granites (Jacob, 1974; Miller, 1983). In its SW termination, the leucogranite also contains xenoliths of a fine-grained, cream-coloured leucogranite. These xenoliths are only found in this SW part of the Stinkbank granite, but they have no larger and coherent equivalent granite phase they can be related to.

5.3.2 Contact relationships and granite geometries

The contacts between the different granite phases are exposed and shown in Figure 5.17, a) and b). Contacts are always sharp and xenoliths are angular. This suggests that little or no assimilation or mingling has occurred between the main melt batches at the emplacement site. It also indicates that earlier granite phases were fully crystallized when later granites were emplaced. Good three-dimensional exposure in this part of the granite allows studying the geometry of the contact zones. The contact between the biotite-rich megacrystic granite and the main leucogranite, in particular, can intermittently be traced over several kilometres in the field. This contact may be sharp and, in all observed cases, the intrusive leucogranite underlies the biotite-rich granite (Figure 5.17 a, b). Alternatively, the contact may be developed as a several meter wide intrusive



Figure 5.17, a) Plan view of the sharp contact between the biotite-rich megacrystic Stinkbank granite (left, strong fabric) and the leucogranite. Note that the leucogranite crosscuts the folded biotite rich megacrystic granite. *b)* Plan view of the sharp contact between the biotite-rich megacrystic Stinkbank granite (left) and the leucogranite (right).

breccia in which angular xenoliths of the biotite-rich granite float within the leucogranite (Figure 5.16 and 5.18). The xenoliths contain a magmatic and solid-state foliation that is similar to the regionally recorded fabric of the biotite-rich megacrystic granite (Figure 5.17). However, this foliation does not show regionally consistent trends and adjacent xenoliths show high-angle internal foliation trends, indicating the rotation of xenoliths in the intrusive leucogranite (Figure 5.18). Importantly, where exposed, this contact shows shallow dips, ranging from near horizontal to ca. 50 degrees (Figure 5.19, a, b). If traced throughout the granite, this contact outlines a gently undulating and folded surface.

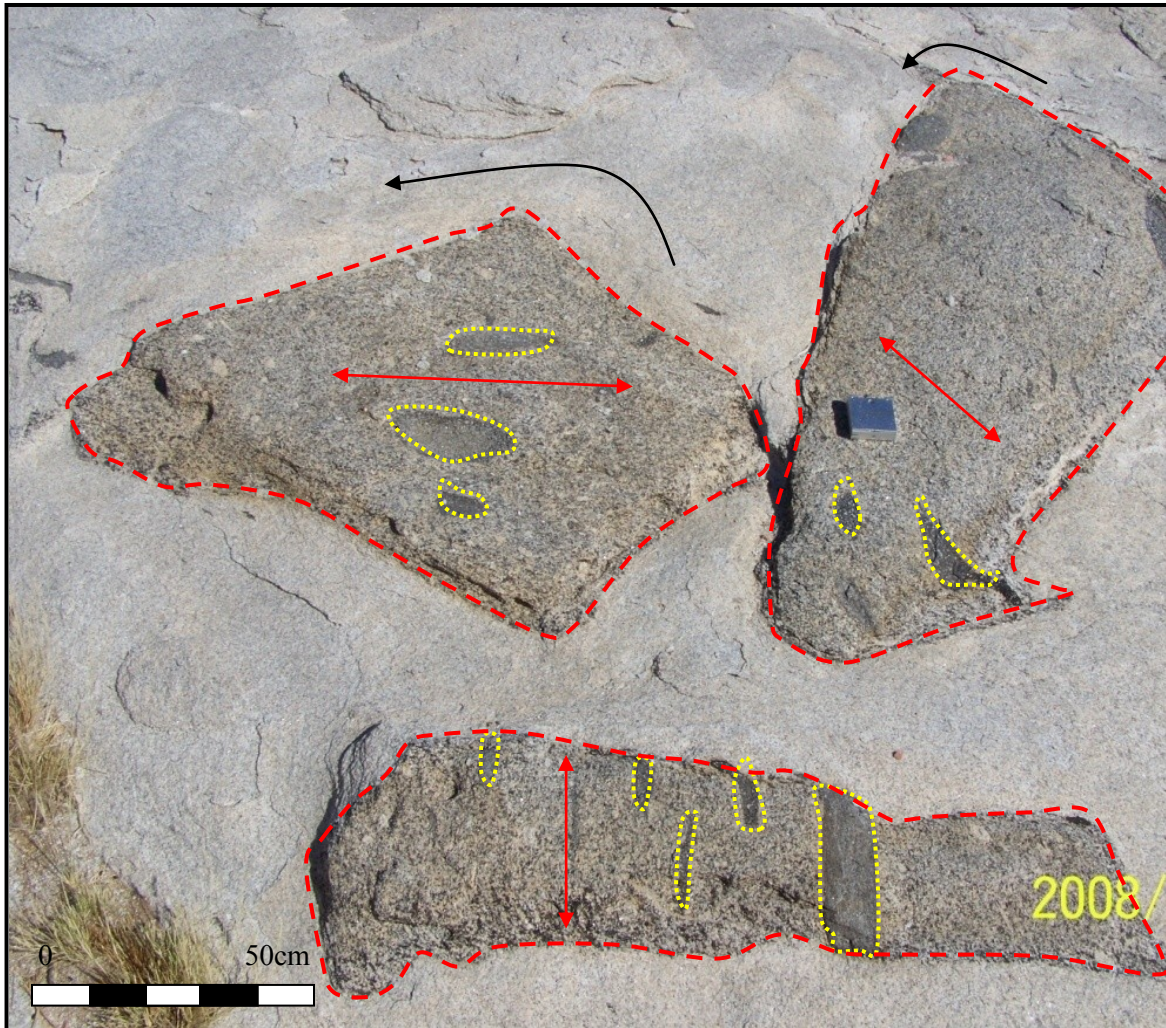


Figure 5.18, Photo taken in plan view. Image shows three large biotite rich megacrystic Stinkbank granite xenoliths (delineated by the red-dashed line) floating within/on top of leucogranite. The foliation S_2 , defined by the alignment of feldspar megacrysts and biotite crystals, is indicated by the red arrows. From the foliation it can be seen that the three xenoliths have been rotated. The biotite rich xenoliths contain small xenoliths of schists and metapelites of the Kuiseb Formation (delineated by the yellow-dashed lines). These internal relationships provide evidence for the timing of the different granites.

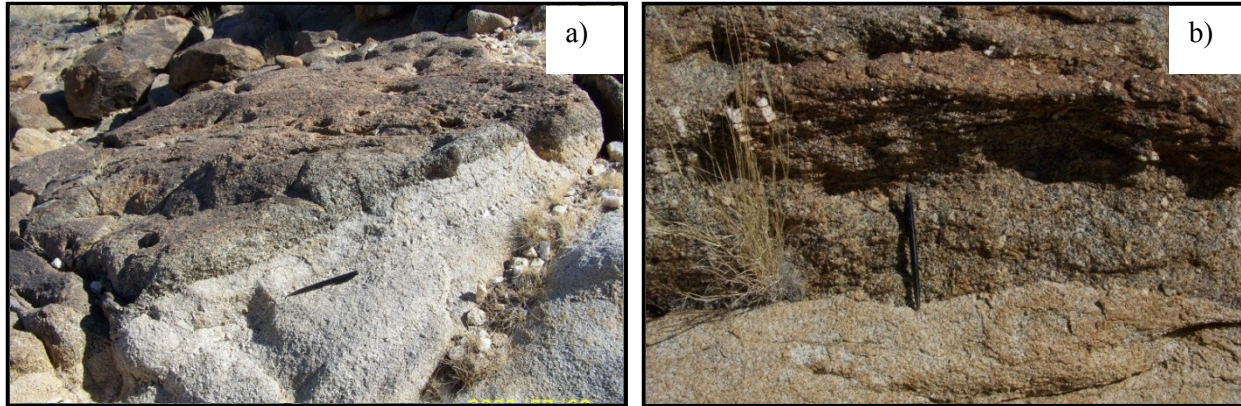
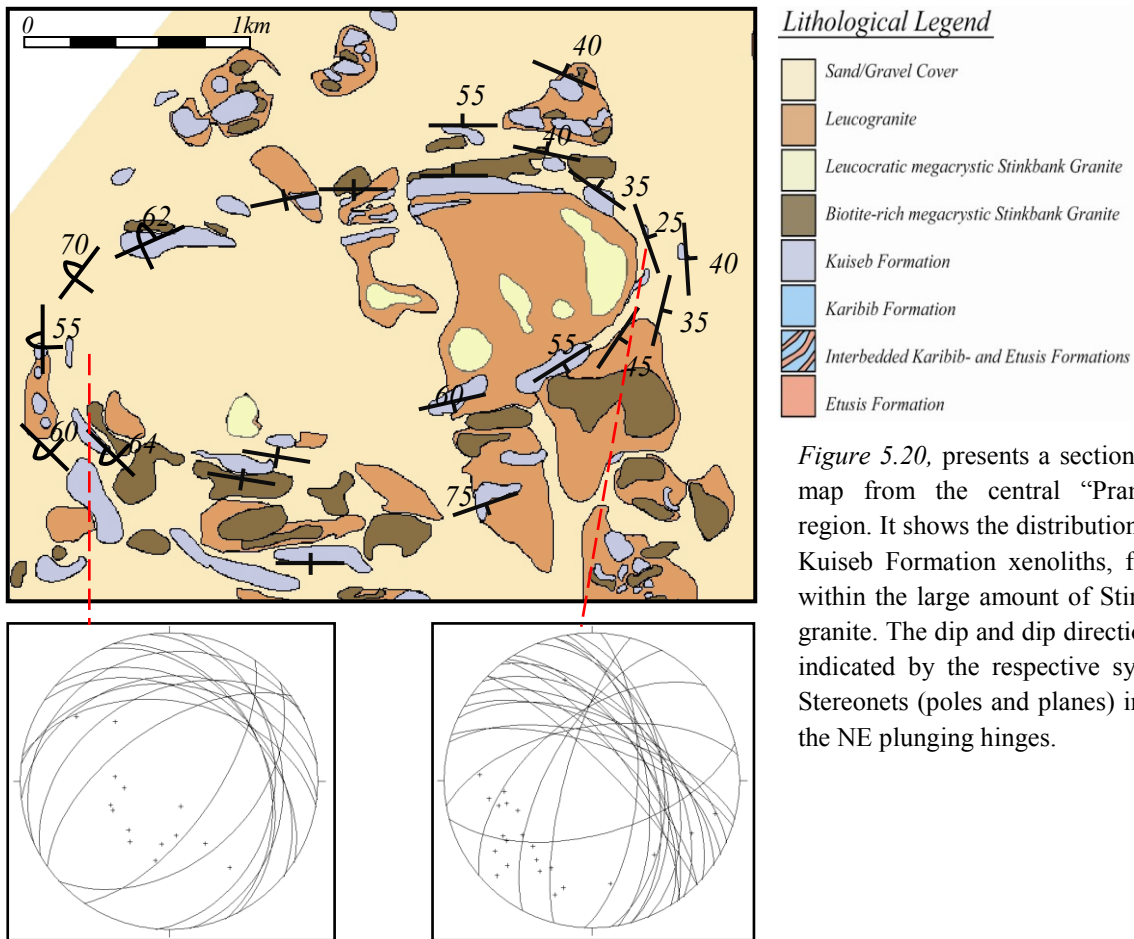


Figure 5.19, a, Oblique view of a shallowly-dipping, sharp contact between the biotite-rich megacrystic Stinkbank granite (top) and the leucogranite (bottom). b) Oblique view of a shallowly dipping contact between the biotite-rich megacrystic Stinkbank granite (top) and the leucogranite (bottom)

The central Pramberg structure, a prominent topographic height extending some 70-80 m above the peneplain centered around coordinates $22^{\circ} 7'55.95''\text{S}$; $15^{\circ}24'54.60''\text{E}$ in the central parts of the Stinkbank granite, illustrates this geometry particularly well. The Pramberg is easily visible on aerial photographs, marked as a NE-trending, in plan ovoid structure, some 4 km along strike and 2.5 km across. It is cored by leucogranite and surrounded by intermittently developed megacrystic leucogranite, followed by biotite-rich megacrystic granite and, finally, wall-rock schists of the Kuiseb Formation. The wall-rock fragments form a train of xenoliths outlining a semi-continuous stratigraphy that can be connected throughout the granite (Figure 5.20). This closely resembles a ‘ghost stratigraphy’ defined by wall-rock fragments and described for many granites worldwide (*e.g. Pitcher, 1979*).

Moreover, the train of country-rock xenoliths wraps conformably around the internal contacts between the biotite-rich megacrystic Stinkbank granite and the leucocratic megacrystic Stinkbank granite in the Pramberg structure. In other words, the orientation of wall-rock xenoliths is parallel to the contacts between different granite phases, indicating the concordant intrusive relationship not only between different granite phases, but also between the granites and the wall rocks. Structural readings of S_0 and S_1 preserved in the xenoliths of the Kuiseb Formation outline a large, NE-trending antiformal structure.



A cross- and longitudinal section illustrates the doubly-plunging, dome-like shape of the central “Prumberg antiform” (Figure 5.21, cross-section and 5.22, longitudinal-section). The orientation of wall-rock fragments and internal granite contacts define a shallowly NE plunging hinge in the NE and a NE plunging hinge in the SW closure of the fold. The latter suggests that the SW hinge is overturned. A similar folding of granite contacts together with the wall-rock ghost stratigraphy can be demonstrated for smaller structures adjacent to the Prumberg (Figures 5.23, 5.24, 5.25). Common to these entire fold structures is that rocks of the Kuiseb Formation are always found to be capping the granites.

Cross-section through the central “Pramberg”

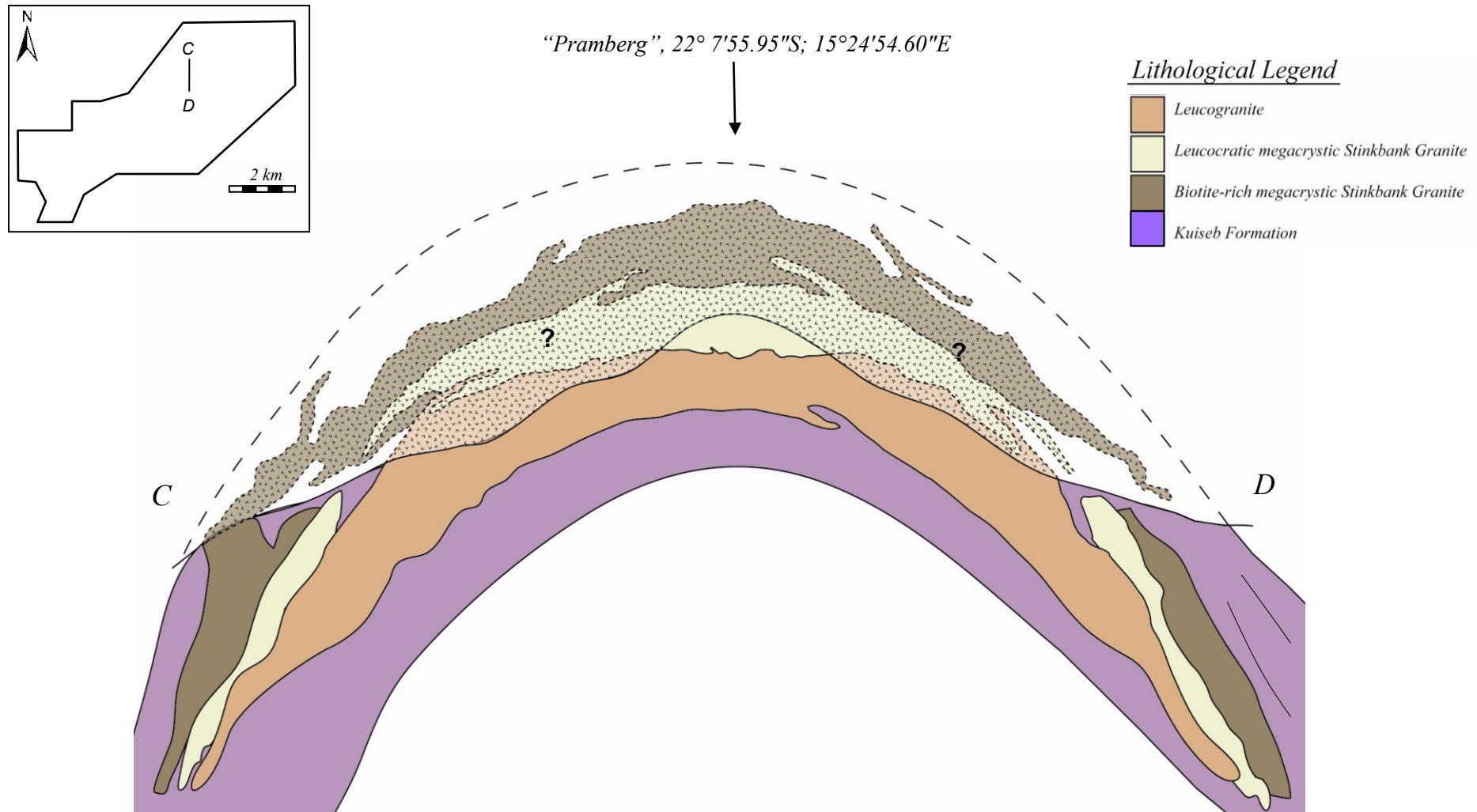


Figure 5.21, Cross-section through the central “Pramberg” area, showing the distribution and dip of sheet-like granite phases and wall rocks outlining an upright, NE-trending antiformal structure. The upright, NE trending fold is parallel to F_2 folds in the surrounding wall rocks (e.g. domain 1). Moreover, the subvertical, NE-trending magmatic and solid state fabrics in the granites are axial planar to the fold and parallel to the S_2 regional fabric in the wall rocks. Vertical exaggeration is 3 X.

Longitudinal section through the central “Pramberg”

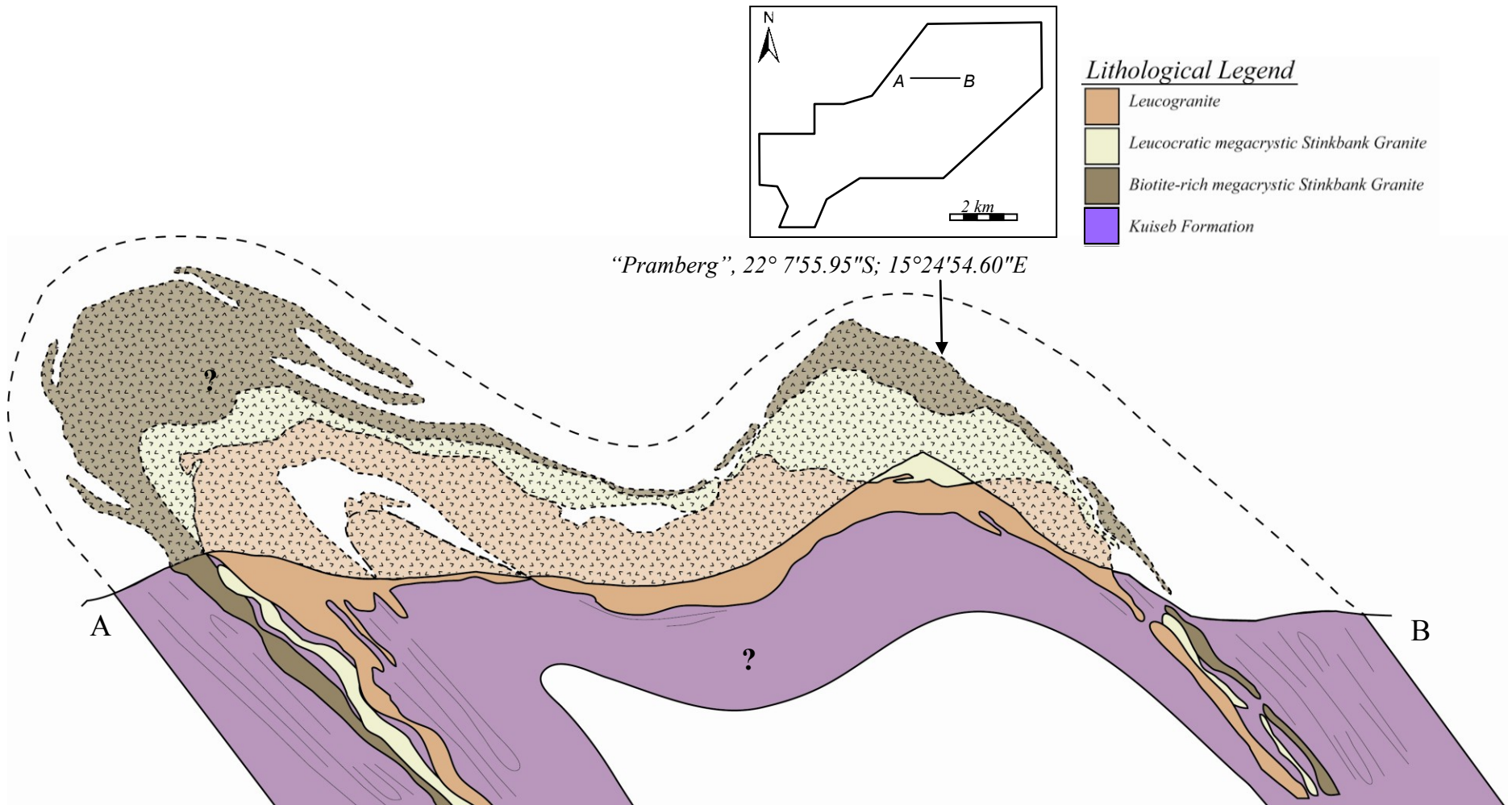


Figure 5.22 Schematic longitudinal section through the central “Pramberg” area. The orientation and distribution of the intrusive granites as well as wall-rock xenoliths of the Kuseib Formation outline the, in general, antiformal geometry of folded granite sheets with a NE plunging hinge in the NE of the structure and an overturned NE plunging hinge in the SW of the Pramberg structure. Vertical exaggeration is 3 X.

Further examples of antiforms within the Kuiseb Formation

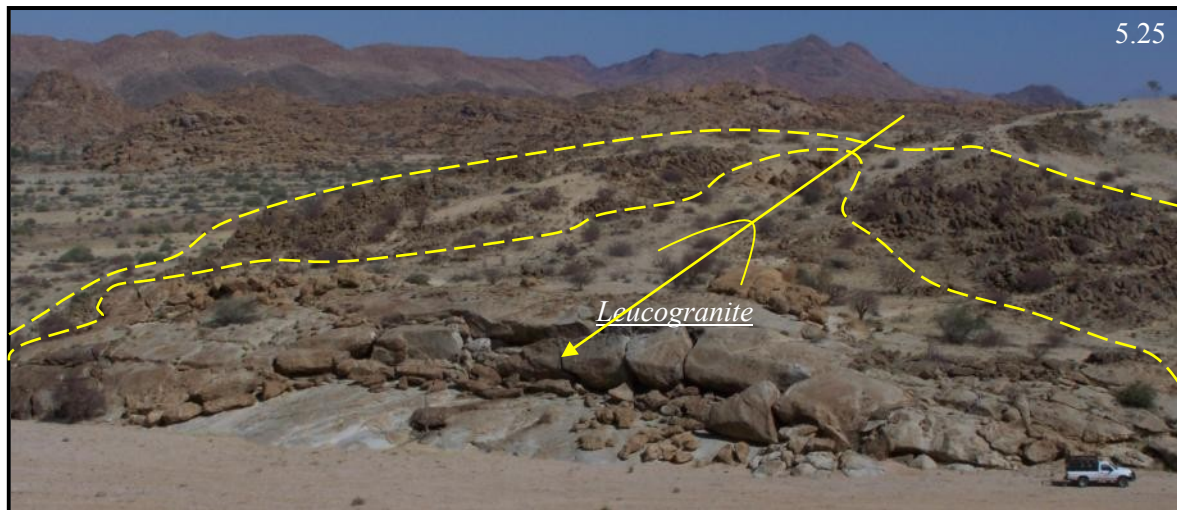
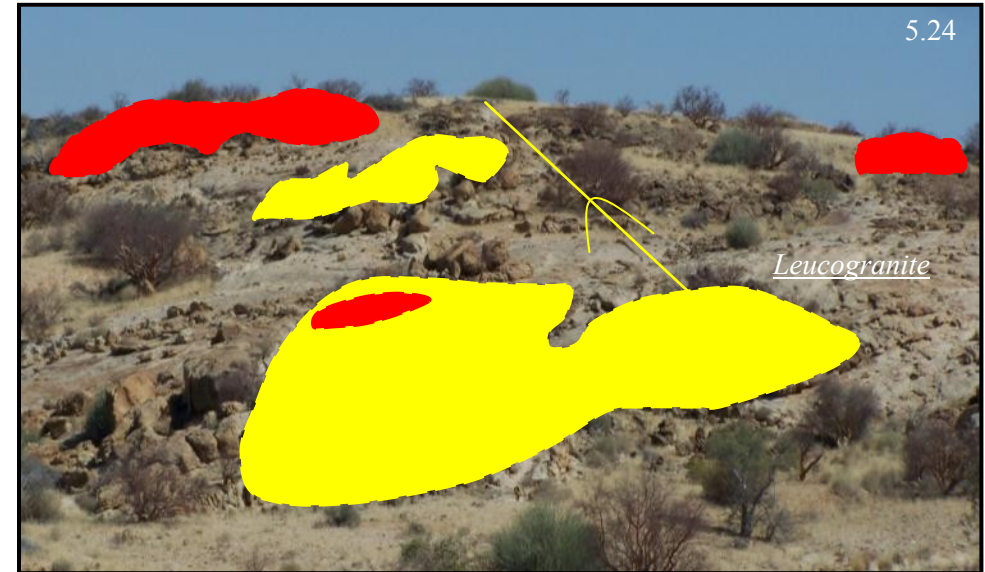
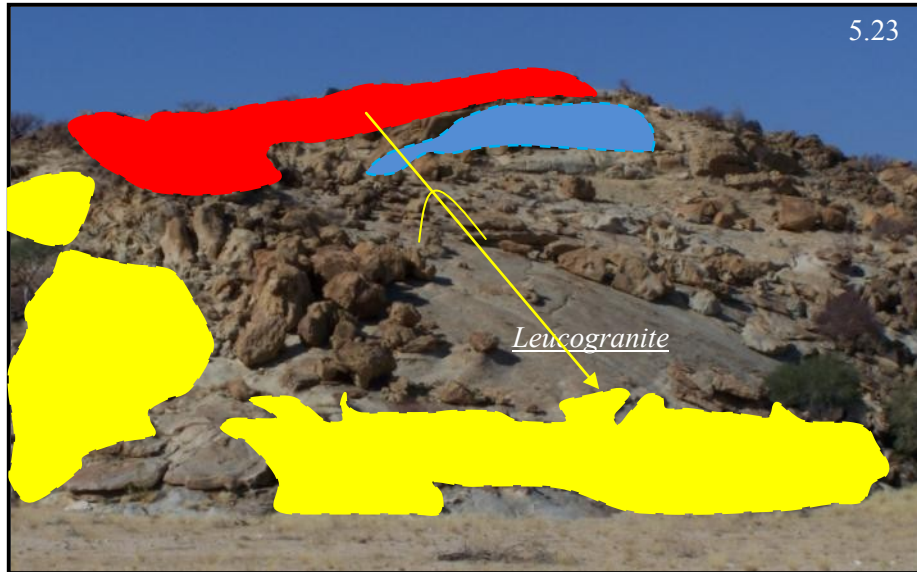


Figure 5.23, 5.24 and 5.25 Oblique views of three individual antiformal structures in the Stinkbank granite, defined by a folded carapace of xenoliths of biotite-rich Stinkbank granite and overlying rocks of the Kuiseb Formation within leucocratic granite. The red areas delineate xenoliths of the Kuiseb Formation; whereas the yellow areas outline the biotite-rich megacrystic granite (blue is a pegmatite). Fold hinge lines annotated for clarity. 5.23, outcrop is 20-30m high, looking NE, fold is plunging shallowly to the SW at 10-20 degrees. 5.24, looking SW, again shows a shallow plunge, this time towards the NE. 5.25, looking towards the SW, shallow dips of 10-20 degrees, fold plunging towards the NE.

Decimeter-sized enclaves of a fine- and even-grained cream-coloured leucogranite are common in SW termination of the Stinkbank granite that is otherwise made up of entirely of the main leucogranite phase (Figure 5.26, a). The enclaves are angular and commonly occur in clusters of closely spaced fragments separated by areas largely devoid of such enclaves. Good exposures of these clusters ca. be found at e.g. 22°10'58.63"S; 15°19'40.07"E and 22°10'50.52"S; 15°19'30.59"E (Appendix 1). These fragments show a preferred orientation, dipping at shallow- to moderate angles to the SW, W and NW, subparallel to the granite-wall-rock contacts (Chapter 4.6). However, the dips in the granite are commonly shallower compared to dips recorded in the wall-rocks (Figure 5.26, b). The orientation of xenoliths plotted throughout the SW termination of the Stinkbank granite defines a moderately SW plunging antiform, subparallel, although shallower, than the antiformal syncline defined by dips of the wall rocks.

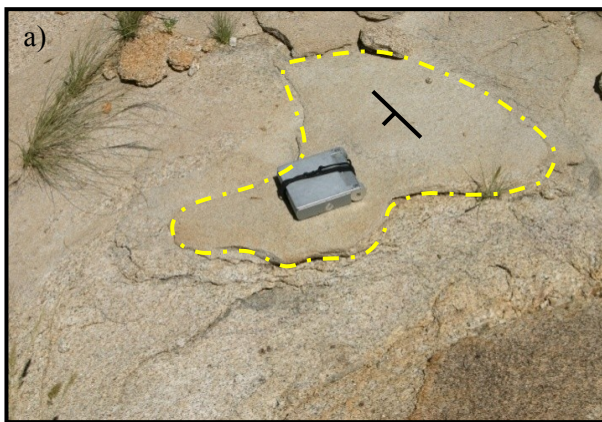
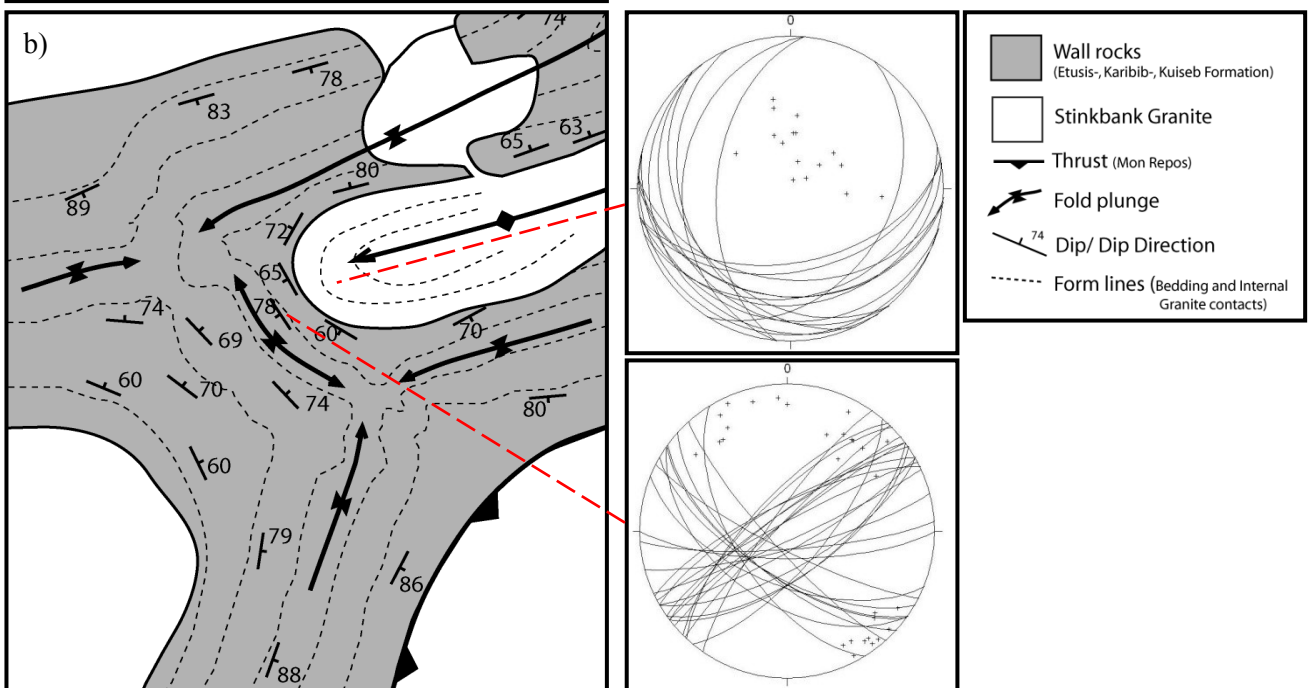


Figure 5.26,

a) Plan view of a xenolith of finer grained leucogranite (above) within and a medium grained leucogranite (bottom).

b) The map insert shows dips of wall-rocks corresponding roughly to the dips of the internal granite contacts between the leucogranite and the fine grained leucogranite. The dips of the internal contacts are generally shallower than those of the wall-rocks.



When the dips of the intrusive contacts are plotted throughout the Stinkbank granite, the contacts can be shown to define a folded surface. Folds show NE trends and commonly double plunges, which, in the case of the Pramberg structure, is even overturned.

In addition, internal contacts between granite phases, particularly the leucogranite is, in places, layered (Figure 5.27). Where observed, the layering illustrates shallow, small folded dips, parallel to the folded contacts between different granite phases.



Figure 5.27, Leucogranite outcrop containing gently folded internal granite contacts. The contacts are generally subhorizontal with shallow internal plunges.

The structural form line map is shown in Figure 5.28, a) Multiple small, doubly-plunging antiformal structures can be seen throughout the field area. These structures are almost always cored by the Stinkbank granites. A cross section, E- F, is drawn throughout the entire field area. It intersects the Pramberg structure and the Kuiseb wall rocks. From the cross section (Figure 5.28, b) the internal sheeting and folding of the granite is clearly illustrated.

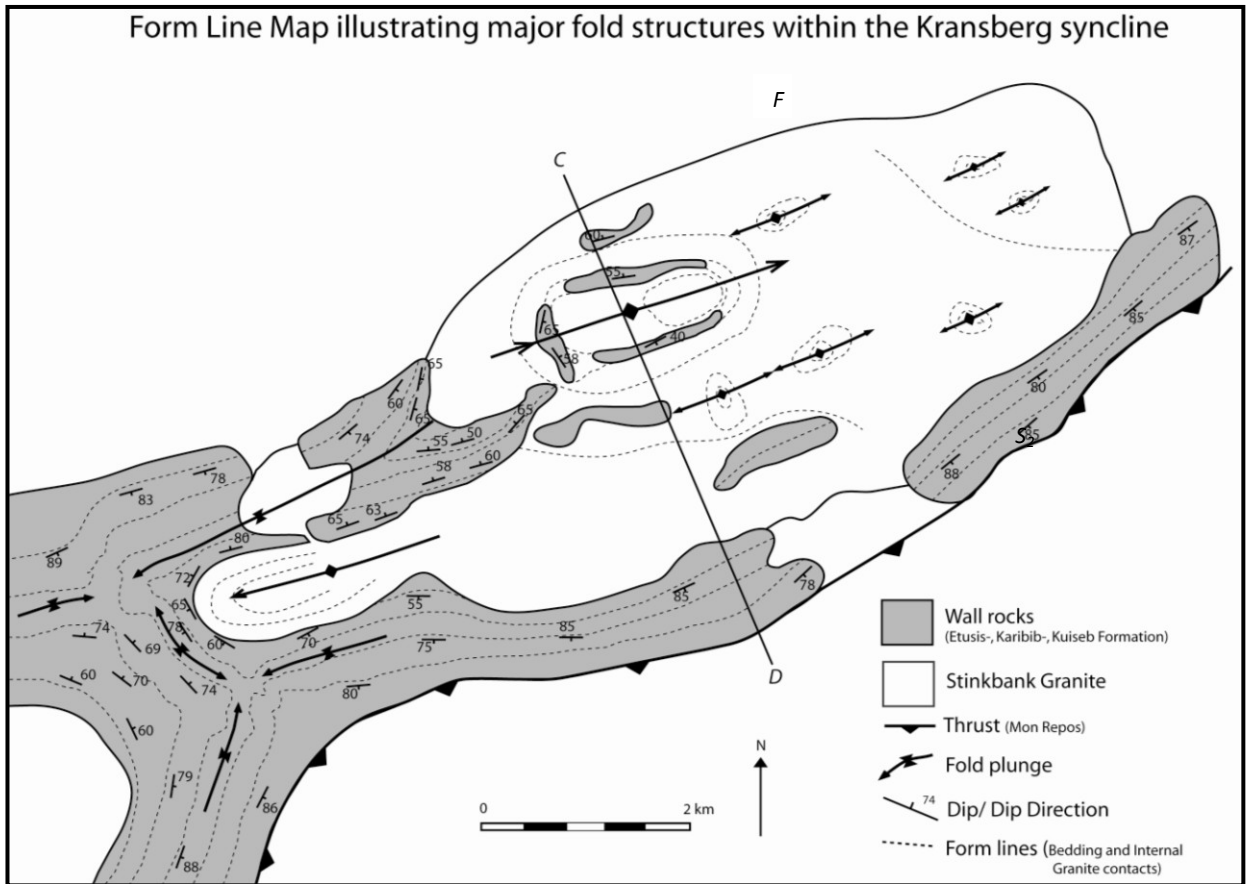
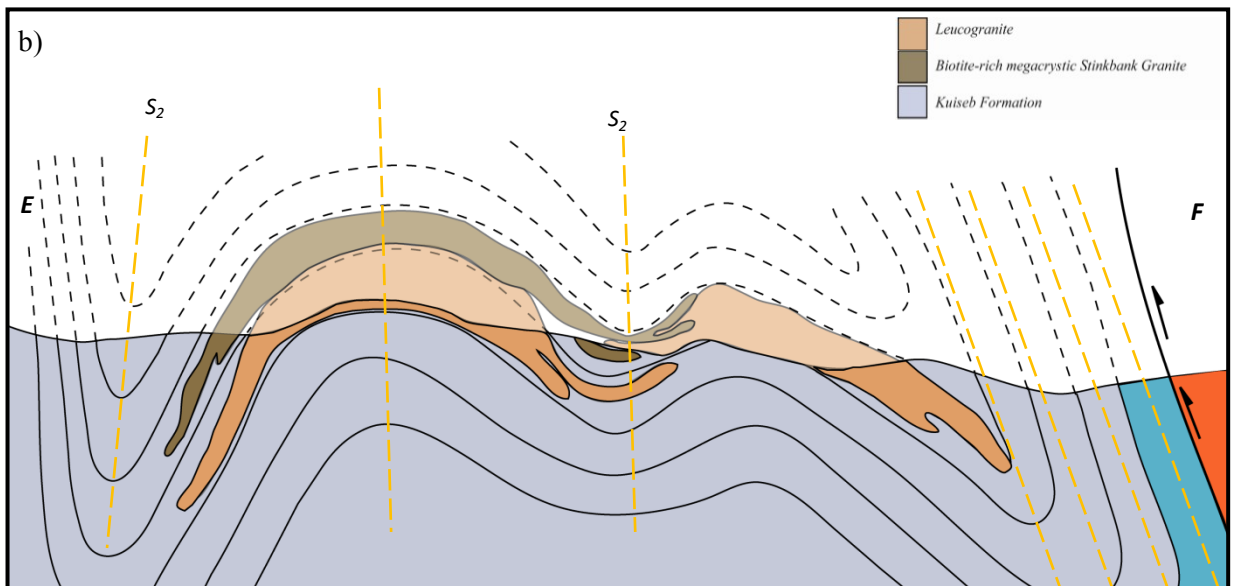


Figure 5.28 a) Form line map illustrating major fold structures within the Kransberg syncline. b) A cross-section E-F drawn through the central part of the Kransberg syncline, it illustrates (a) the folded nature of the sheet-like granite phases and (b) the antiformal nature of this part of the Kransberg syncline. The Biotite-rich megacrystic granite and the leucogranite can be seen intruding concordantly, as sheets, within the Kuiseb Formation.



5.3.3 Granite Pseudostratigraphy

The cross- and longitudinal sections also illustrate a relative intrusive stratigraphy between different granite phases, at least in the central parts of the Stinkbank granite, where all phases are developed. In this sequence, the biotite-rich megacrystic granite forms the structurally upper unit, intruding into and brecciating rocks of the Kuiseb Formation. The leucocratic megacrystic granite intrudes below the biotite-rich granite, although its development is rather patchy and more localized. The leucogranite occupies the stratigraphically lowest portions and is, thus, mainly exposed in the cores of the antiformal structures. Xenoliths of e.g. the biotite-rich megacrystic granite define a relatively smooth, gently folded surface, showing little or no evidence of up- or downward movement of blocks, although blocks may be rotated against each other. This again indicates the sheet-like geometry of the granites. It also points to a distinct asymmetry between the upper and lower contacts of the granite sheets. The lower contacts are relatively sharp. The upper contacts of the sheets, in contrast, show a brecciation of the wall rocks, resulting in e.g. xenoliths of Kuiseb Formation in the biotite-rich granite, or fragments of biotite-rich granite in the structurally lower leucogranite (Figure 5.29). Pegmatites are also commonly found at a certain ‘stratigraphic’ position, and up to 5 m thick lensoid pegmatite bodies can be seen to be capped by the Kuiseb Formation, at or along the contact with the intrusive biotite-rich megacrystic granite.

Different to this pseudostratigraphy in the central part of the Stinkbank granite is the intrusion of the leucogranite along the SE and SW contacts. Here, the granites are in direct contact with the wall rocks and the biotite-rich granite seems to be absent.

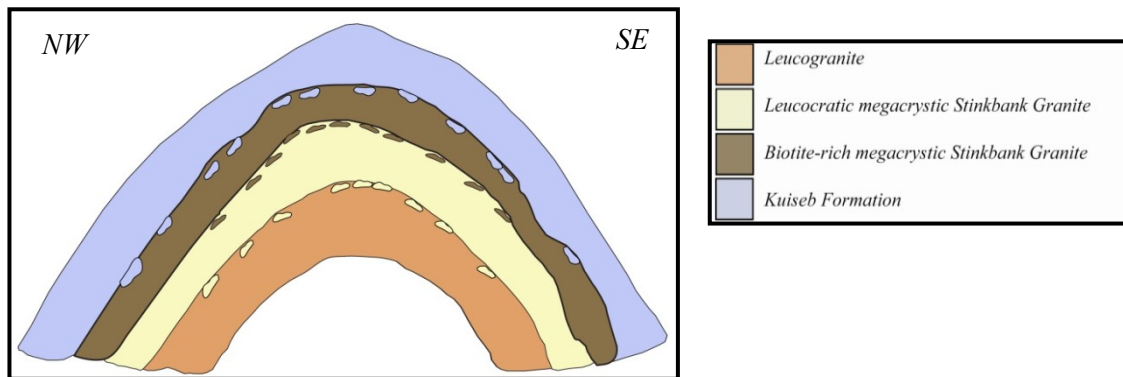


Figure 5.29, Schematic cross section through a characteristic antiformal structure within the central portion of the Stinkbank granite, illustrating the sheet-like nature of the granites and the ‘pseudostratigraphy’ between different granite phases. The top contacts of individual phases are commonly brecciated against the overlying older granite phases and/or wall-rock. Vertical scale has been exaggerated.

5.3.4 Granite- Wall rock contacts

Granite wall-rock contacts are variable throughout the field area and vary from concordant with the bedding and/or foliation of the wall rocks to highly discordant and sharply cross-cutting. Concordant versus discordant contacts seem to mainly be a function of the scale of observation. On a regional scale, the Stinkbank granite shows largely concordant wall-rock contacts having intruded in a bedding-parallel fashion. On a more local scale, contacts can be seen to be discordant, either in the form of cross-cutting granite sheets interfingering with the wall rocks or the through the separation and stoping of country rocks along discordant and, in places, high-angle apophyses and sheets.

Concordant wall-rock contacts are evident along the SE margin of the Stinkbank granite as well as large parts of the SW termination of the Stinkbank granite. Intrusive and contact relationships are well exposed in a number of river sections in the Khan River and tributaries to the Khan River that cut at high angles through the contact. Here, the contact can be seen to be dipping between 60-70 degrees to the SE and S, respectively, with the granite concordantly underlying the schists of the Kuiseb Formation (Figure 5.30). This contact can be followed, at least intermittently, for 6-7 km along strike between the farm Safier (22°10'35.65"S; 15°23'18.96"E) and close to the SW termination of the Stinkbank granite.

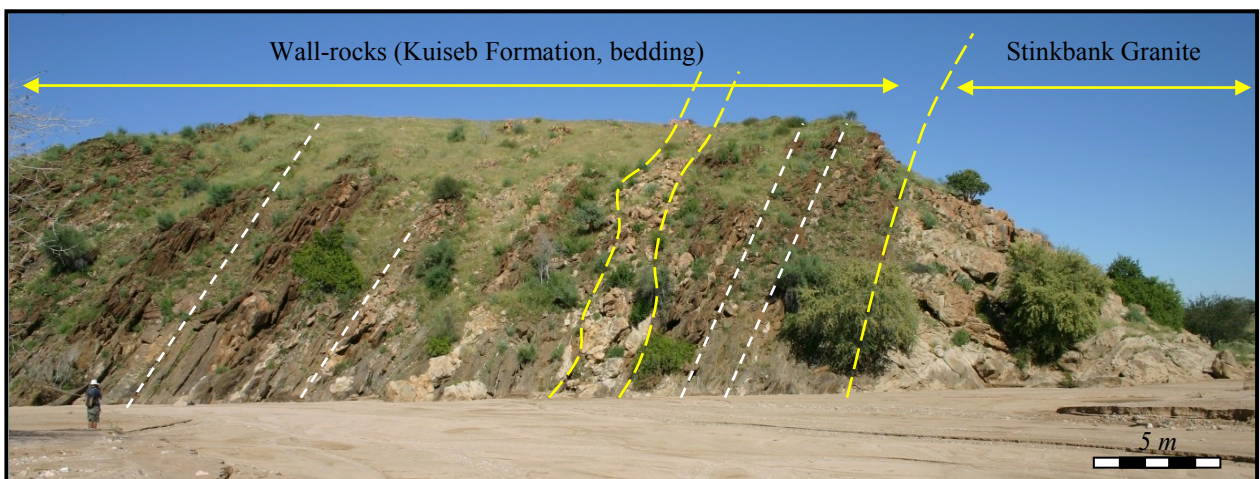


Figure 5.30, River cutting (Khan River) along the S- limb of the Kransberg syncline, illustrating the concordant contact between the Stinkbank leucogranite and the Kuiseb wall-rocks. The contact is sharp with very few wall-rock fragments seen within the leucogranite. A bedding parallel sill is indicated by the dashed yellow line, approx 10 meters from the granite- wall-rock contact. Looking SW, along strike of the granite and wall-rock contact. Note the boudinage of smaller sills in the wall rocks.

The SW termination of the granite is characterized by the sharp change of strike of the contact to more northerly trends, also marking the antiformal closure of the Kransberg syncline. Dips are at moderate- to steep angles (40-65°) to the SW, W and NW. This contact is, on a scale of hundreds of meters, concordant and the granite underlies rocks of the Kuiseb Formation. In detail however, this contact shows a somewhat serrated geometry. This geometry is the result of low-angle (5-15°), wedge-shaped apophyses that interfinger with the overlying wall rocks (Figure 5.31).

The apophyses are thicker (5-20m) where they are connected to the granite and tend to pinch away from the granite wall-rock contacts, some 100-200m along strike (Figure 5.31). The overall effect is the, in detail, irregular granite wall-rock contact. While the wedge-shaped apophyses appear to prize off wall rocks, the underlying granite is devoid of wall-rock xenoliths that would indicate this type of stoping. Granite sheets in the overlying wall rocks are predominantly bedding-parallel sills, with only very subordinate cross-cutting dykes.

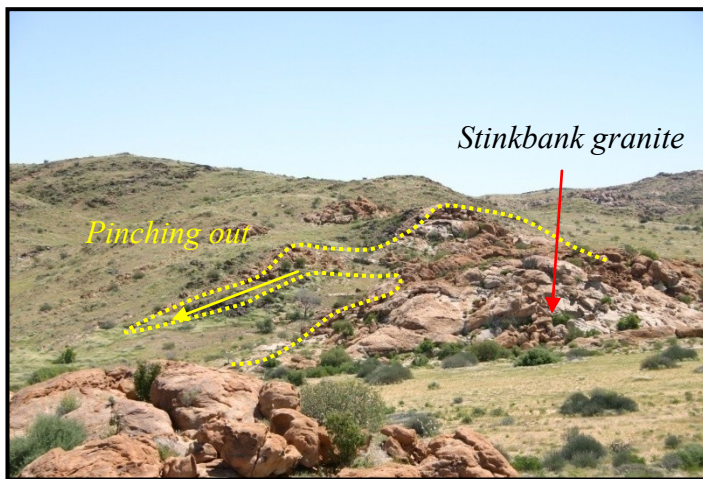


Figure 5.31, Looking W, across the southern closure of the Kransberg syncline showing granite apophyses within the wall-rocks. The apophyses are thicker (5-20m) where they are connected to the granite and tend to pinch away from the granite wall-rock contacts, some 100-200m along strike. The overall effect is the, in detail, irregular granite wall-rock contact. The contact dips at 50-60° away from the view of this photo.

Granite sheeting is not locally observed in the otherwise homogeneous leucogranite (Figure 5.27) and the alignment of xenoliths (Figure 5.26, b) indicates largely concordant internal contacts within the granite compared to the wall rocks. The only difference is that dips of the xenoliths in the granite tend to be shallower compared to dips of the wall rocks. Further to the N, contacts between the leucogranite and wall-rocks become increasingly more discordant. This is particularly evident where the leucogranite sharply truncates a large, second-order NE trending synform. The actual contact relationships are, however, not exposed in this part of the granite.

Despite the largely concordant granite wall-rock contact relationships, discordant contacts are common on a smaller scale (meters to tens of meters). The presence of large, angular wall-rock xenoliths, up to several hundred meters in strike extent, also indicates sharply cross-cutting contact relationships. These xenoliths are particularly common along the south-central parts of the Stinkbank granites (22° 9'25.61"S; 15°25'16.79"E, Appendix 1) (Figure 5.32).

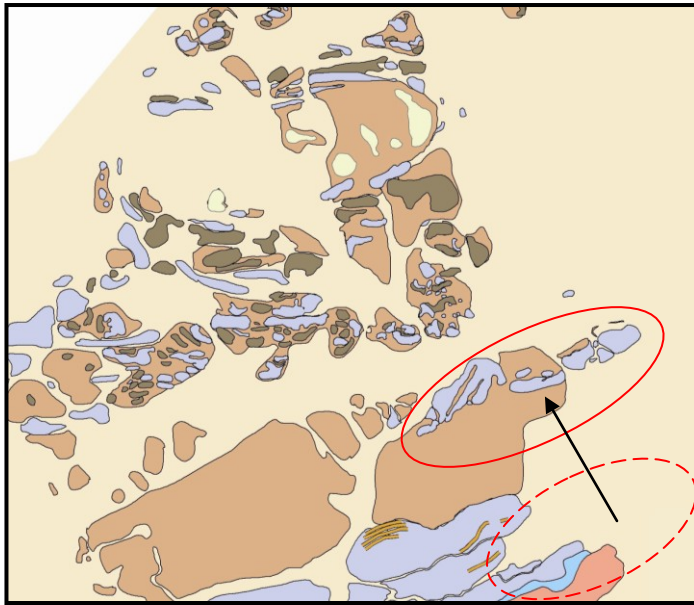


Figure 5.32, Map detail of the contact between the leucogranites and wall rocks of domain 1, showing the separation of large, km-sized country-rock xenoliths from the wall rocks of the Kuiseb Formation.

Larger wall-rock xenoliths commonly contain bedding-parallel granite and pegmatite sills, similar to those found in the wall rocks. This indicates that at least parts of the granite sheeting observed in the wall rocks pre-dated the main phase of leucogranite intrusion and eventual incorporation of wall rocks into the main body of the granite. The partial or complete assimilation of wall rocks by the granite, as described for numerous occurrences of other Salem-type granites (*e.g. Jacob, 1974; Miller, 2008*) is not observed in the Stinkbank granite.

The processes of wall-rock stoping of fragments seems well preserved along parts of the granite wall-rock contacts. These contacts describe a progression from (1) in-situ wall rocks, i.e. wall rocks that have been intruded by intersecting high-angle granite sheets, but that are fully attached to the wall rocks, via (2) wall rocks that are completely surrounded by granite, but have not been incorporated by the granite and/or dislodged from the wall rocks, to (3) angular wall rocks within the main body of the Stinkbank granite, undergoing various degrees of rotation and not showing any obvious connection to the adjacent wall rocks. The progressive separation or stoping of wall rocks occurs via two to three sets of intersecting high-angle granite sheets. Bedding-parallel sills

are the first and most prominent sheet geometry that is present throughout the wall rocks of the Stinkbank granite (Figure 5.33, a). A second set of high-angle granite sheets forms initially as short, isolated veins in boudin necks or extension fractures at high-angles to the shallowly NE and SW plunging mineral stretching lineation. These veinlets are initially confined to more competent lithologies, but can be seen to dilate and cross-cut entire meter-wide packages. The right-angle intersection of bedding-parallel sills and high-angle sheets creates ladder-type structures (Figure 5.33, b) and an almost rectangular or box-like geometry of fragments (Figure 5.34 and 5.35) that also characterizes xenoliths in the interior of the Stinkbank granite. The final separation of wall rocks occurs when low-angle, cross-cutting dykes truncate the sequence, following which the wall rocks are completely surrounded by intersecting high-angle granite sheets.

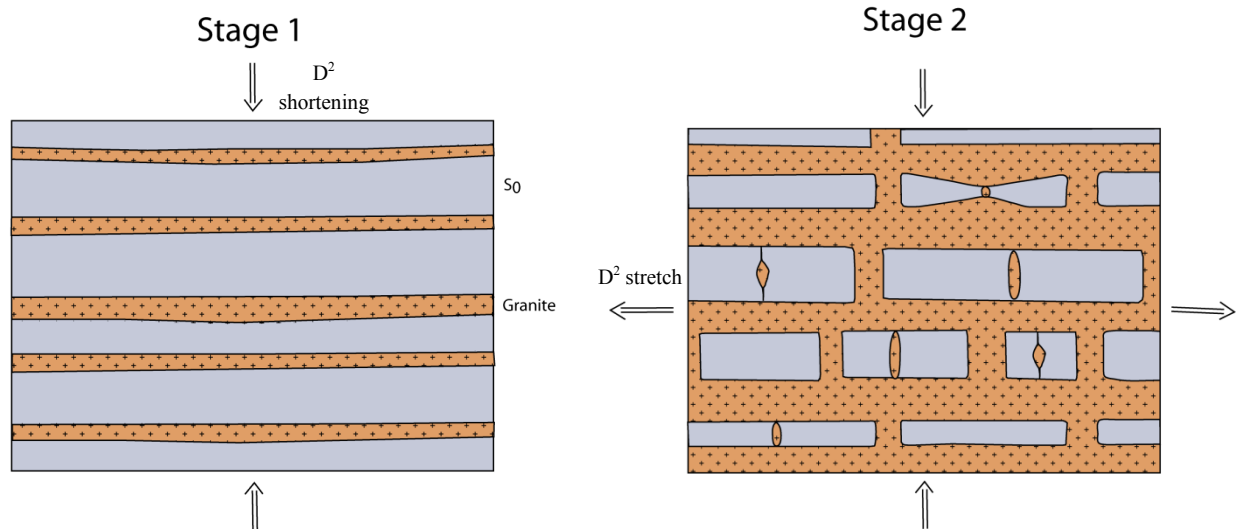


Figure 5.33, a) Stage one of the progressive separation of wall rocks is signified by the intrusion of bedding parallel sills. These sills amalgamate to form larger sills.

b) Stage two is characterized by the intrusion of a second set of high angle granite sheets. Initially they are seen as short, isolated veins within boudin necks. These small veinlets then expand by further granite intrusions. The intrusion of two or three different sets of sills cause the formation of box-like fragments or xenoliths.

Rotation of fragments and wall-rock separation occurs upon the progressive dilation of one or more of the sheets or the repeated emplacement of granite sheets. Depending on the width of the granites, and the relative spacing between the intruding sheets, the size of these xenoliths can range from centimetre- to hundreds of meters in width and strikelength.

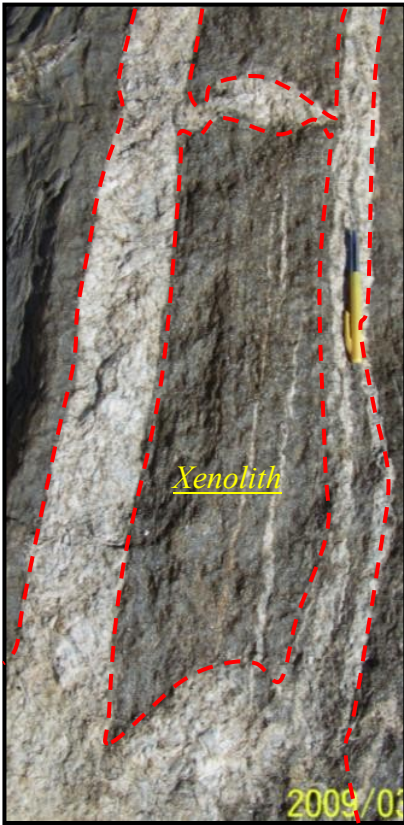


Figure 5.34, left, Oblique plan view of a developing ladder structure made up of connecting bedding-parallel sills and high-angle, cross-cutting dykes (extension fractures filled by granite). The resulting shape of the “future” xenolith is highly angular and box-like.

Figure 5.35, top, Oblique view of a larger Kuiseb xenolith showing the effects of progressive dilation and/or multiple intrusion of granite sheets for the separation of wall rocks. High-angle cross-cutting sheets are indicated by the yellow, dashed line, connected to bedding-parallel sills at the top and bottom of the xenolith. Dilation in the cross-cutting sheets is indicated by red arrow. Note the presence of high-angle boudin necks and extension fractures parallel to the cross-cutting sheets.

6. GEOCHEMISTRY

The three mineralogically distinct phases of the Stinkbank granite, namely the biotite-rich megacrystic granite, the leucocratic megacrystic granite and the leucogranite have also been described for other occurrences and are, in fact, a hallmark of the Salem-type granites in the Damara Belt (*Jacob, 1974; Miller, 1983; Jung et al, 1998*). These works have also described gradational contacts between the granite phases and the granites and wall rocks of the Kuiseb Formation, extensive wall-rock assimilation and in-situ differentiation (see summary in *Miller, 2008*). All these processes are inferred to have affected the composition of the Salem-type granites. This chapter is intended to provide a brief characterization of geochemical differences between the granite phases that may also point to the origin of the granites, but an in-depth geochemical treatment of the data is beyond the scope of this study.

Granitoid classification is based upon the principle that the granite geochemistry reflects the source of the granites so that different granite compositions may reflect contrasting source rocks (*e.g. Clemens, 2003*). The question arises as to whether the compositionally very distinct and spatially closely associated granite phases of Salem-type granites represent the final emplacement of chemically distinct granites, possibly tapping different sources in the deeper Damara crust, or whether other processes at or close to the emplacement site have to be invoked for the compositional heterogeneity. The broad classification of granites into I- and S-type granites (*e.g. Chappell and White, 1974, 2001*) uses geochemical and petrological evidence to distinguish potential source rocks in the deeper parts of orogens that may undergo partial melting. I-type granites mainly result from partial melting of mafic- to intermediate, meta-igneous crustal rocks. S-type granites, in contrast, form by partial melting of predominantly aluminous sediments. Both show chemical and mineralogical characteristics and these will be briefly presented and then discussed for samples of the Stinkbank granites in the following chapter.

For this purpose, five samples of the biotite-rich megacrystic Stinkbank granite, leucocratic megacrystic Stinkbank granite and four samples of the leucogranite were taken. The rocks were individually crushed to a 1- 2 cm grain size. These grains were then crushed to fine sand in the “teddy bear” crusher. The final step was the grinding of this sand to an even finer powder, by placing it in a carbide-tungsten mill for a total of 1 minute. The 14 powders were sent to the University of Hamburg in Germany where the XRF analyses were carried out.

The finely ground (< 63µm) sample powders were precisely weighed into platinum crucibles with a sample/flux ratio of 1:6 and subsequently homogenized. Glass beads were prepared on a part-automatic burner with 6 individual burners to secure complete oxidation and fluxing of the samples. Analyses were performed on a fully automated wavelength dispersive X-ray fluorescence spectrometer MagixPRO from Pananalytical® attached to a fully automated sample holder PW 2540 VCR with an Rh anode. Accuracy and precision was monitored using international rock standards. For major elements, the measured values agreed within 1-2% relative to the recommended values depending on concentration. For most trace elements, the measured concentrations agreed within 5-20% depending on concentration (> 100 ppm: 5%; 10-100 ppm: 10%, < 10 ppm: > 20%). Detection limits for major elements are 0.01 % for Na and Mg and < 0.01% for the rest of the elements. For the trace elements, detection limits are 20 ppm for Ce and La, 15 ppm for Co, 10 ppm for Ba and Nd and 5 ppm for the rest of the elements. Detection limits are approximate values based on large number of analyses of international standards. Note that matrix effects, measurement times etc. may influence these values. The results are listed in the tables 6.1 and 6.2 below. **LG**: Leucogranite; **LS**: Leucocratic megacrystic Salem type granite; **DS**: biotite-rich megacrystic Stinkbank granite.

Table 6.1 Samples and corresponding major element values given in weight %

Samples	SiO ₂	Al ₂ O ₃	Fe ₂ O ₃	MnO	MgO	CaO	Na ₂ O	K ₂ O	TiO ₂	P ₂ O ₅	unit
LG 1	72.99	13.24	2.33	0.03	0.11	0.94	2.64	5.71	0.32	0.1	%
LG 2	72.61	13.7	1.91	0.03	0	0.9	2.89	5.64	0.25	0.15	%
LG 3	72.46	13.39	1.97	0.03	0.21	1.03	2.81	5.33	0.26	0.15	%
LG 4	72.22	13.5	2.12	0.03	0.1	1.01	2.84	5.29	0.28	0.18	%
LS a	70.66	14.69	2.69	0.05	0.37	1.98	3.45	4.26	0.37	0.26	%
LS b	71.67	14.59	1.9	0.04	0.14	1.56	3.27	5.36	0.26	0.1	%
LS c	72.33	13.77	2.43	0.05	0.23	1.77	3.32	3.87	0.33	0.11	%
LS d	74.05	13.49	2.31	0.04	0.26	1.6	3.12	4.19	0.32	0.1	%
LS e	73.45	13.95	3.18	0.05	0.39	1.62	2.86	4.26	0.48	0.25	%
DS a	63.39	15.78	6.17	0.09	1.81	3.31	3.07	3.66	1.06	0.29	%
DS b	63.25	15.88	5.91	0.1	1.73	3.44	3.28	3.06	1.05	0.28	%
DS c	66.85	15.44	4.41	0.07	1.29	2.6	3.4	3.24	0.7	0.21	%
DS d	66.52	15.42	4.93	0.08	1.57	2.82	3.07	3.68	0.77	0.21	%
DS e	67.02	15.75	4.36	0.08	1.21	3.01	3.5	3.09	0.7	0.21	%

Table 6.2 Samples and corresponding trace element values given in ppm

#	Ba	Ce	Cr	Cu	Ga	La	Nb	Nd	Ni	Pb	Rb	Sc	Sr	Th	U	V	Y	Zn	Zr
LG 1	346	165	3	0	14	82	24	66	7	46	284	7	85	58	3	20	22	48	195
LG 2	352	108	3	0	17	50	24	44	0	46	379	8	79	42	7	9	27	56	158
LG 3	323	108	3	0	13	47	24	37	6	46	355	0	63	49	3	12	27	56	148
LG 4	300	127	1	1	15	56	29	55	12	48	360	6	75	49	9	22	28	61	154
LS a	408	61	3	0	11	34	17	24	11	41	210	5	112	20	6	27	29	57	183
LS b	556	62	6	0	13	21	13	24	9	43	220	3	115	19	9	23	15	42	124
LS c	337	61	0	2	16	39	16	22	8	36	190	8	108	28	5	31	19	52	146
LS d	367	68	0	15	10	24	16	27	10	36	198	11	106	27	6	27	17	49	142
LS e	488	73	4	3	15	39	21	28	10	33	228	6	124	24	5	30	18	59	216
DS a	851	104	23	37	15	50	27	51	18	26	212	13	261	17	0	95	29	94	335
DS b	791	99	14	25	20	60	30	43	18	27	222	10	259	20	1	85	32	92	322
DS c	644	123	18	28	21	60	21	50	19	27	252	9	163	24	2	75	34	78	269
DS d	738	130	21	29	17	79	20	47	21	30	215	7	178	31	5	81	33	84	270
DS e	716	99	17	14	16	48	18	40	16	23	209	11	186	18	5	75	28	83	227

6.1 Results

Major element abundances show a relatively large variation (e.g. SiO₂ 63-73wt%; Fe₂O₃ 2-6 wt%; CaO 1-3.5 wt %) for the Stinkbank granite as a whole. However, major element variations are much narrower within individual phases and there is a clear distinction between the biotite-rich Stinkbank granite (lower SiO₂ and K₂O, higher Fe₂O₃, MgO and CaO) and the more leucocratic varieties. Similarly, consistently higher Cr, Cu, and Sr values (Sr in biotite and the more calcic plagioclase) in the biotite-rich megacrystic granite reflect the distinct mineralogy of the granite phases. The TAS diagram distinguishes plutonic rocks based on their major element values, Na₂O+K₂O vs. SiO₂ (Figure 6.1). Figure 6.1 shows that the biotite-rich megacrystic Stinkbank granite (●) plots into the field of granodiorites, while the leucogranite (▲) and the leucocratic megacrystic Stinkbank granite (■) plot in the granite field.

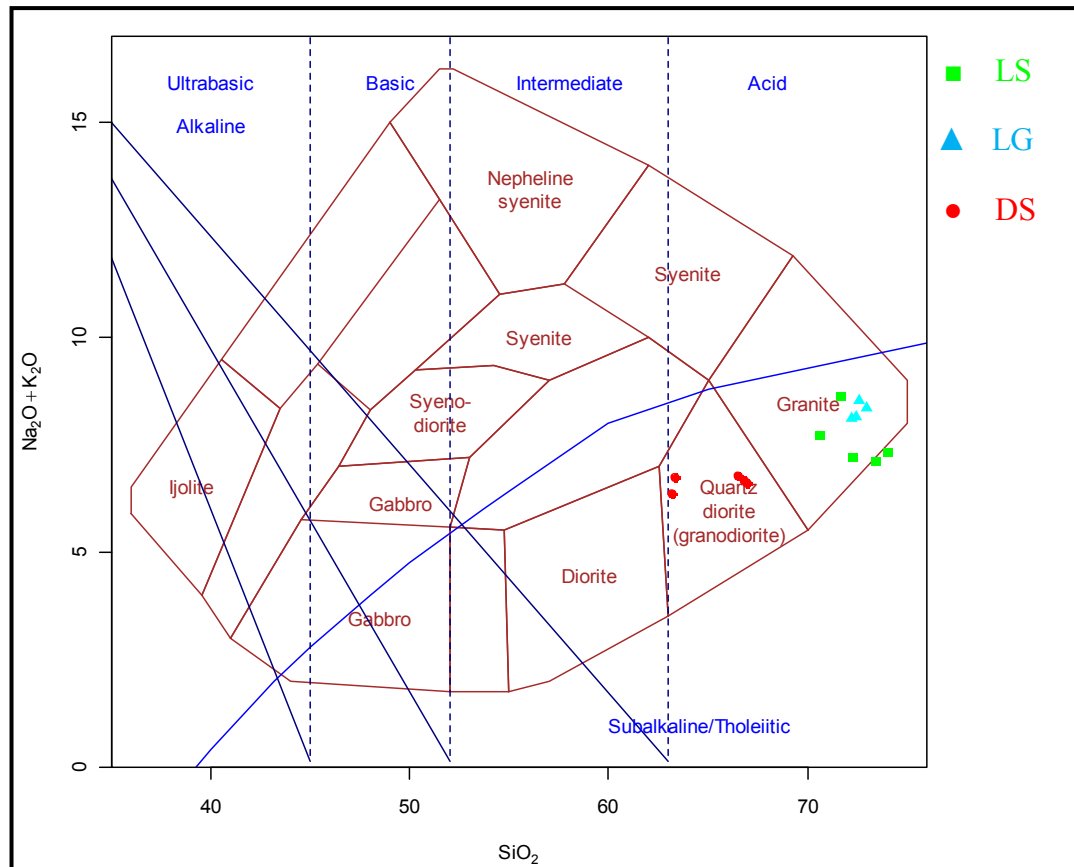


Figure 6.1, Classification plot (TAS) with SiO₂ on the x axis and Na₂O+K₂O on the y-axis. Plot shows the biotite rich megacrystic Stinkbank granite is a granodiorite, while the leucogranite and leucocratic megacrystic Stinkbank granite both plot as granites (sensu stricto). (Cox *et al.*, 1979; Janousek *et al.*, 2006)

A commonly used discriminator between S- and I-type granites is the aluminium saturation index (ASI; $Al_2O_3 / (Na_2O + K_2O + CaO)$), using molecular amounts (converted from weight %). Because of their lower Ca and Na contents, S-type granites are commonly oversaturated in Al, resulting in higher ASI values compared to I-type granites. In their study of granites from the Lachlan Fold Belt, Chappell and White (1974) analyzed hundreds of granite samples and distinguished S- from I-type granites at an ASI index of ca. 1.1 (S-type ASI > 1.1; I-types ASI < 1.1). However, Chappell (1999) also pointed out that there is an overlap between relatively felsic, unfractionated I-type granites with values at around 1-1.1 and S-type values that may fall within the range of 1-1.25, so that a clear distinction based on the ASI value only is not always possible. Table 6.3 lists and Figure 6.2 shows an ASI plot of all 14 samples of the Stinkbank granite. ASI values plot close around 1.1, ranging between 1.04 and 1.14. ASI values for the

leucogranite cluster very closely at around 1.1, those for the biotite-rich Salem-type granite are marginally lower. The megacrystic leucocratic granite shows the largest range with ASI values between 1.04 and 1.14. Hence, the ASI values for the Stinkbank granites seem inconclusive with regard to a distinction of different phases.

Table 6.3, ASI values for the 14 samples.

	<i>Label</i>	<i>ASI</i>
LG 1	LG	1.08232
LG 2	LG	1.09638
LG 3	LG	1.09173
LG 4	LG	1.10343
LS a	LS	1.04082
LS b	LS	1.07001
LS c	LS	1.07257
LS d	LS	1.13769
LS e	LS	1.04986

	<i>Label</i>	<i>ASI</i>
DS a	DS	1.06129
DS b	DS	1.11659
DS c	DS	1.08889
DS d	DS	1.08058
DS e	DS	1.05783

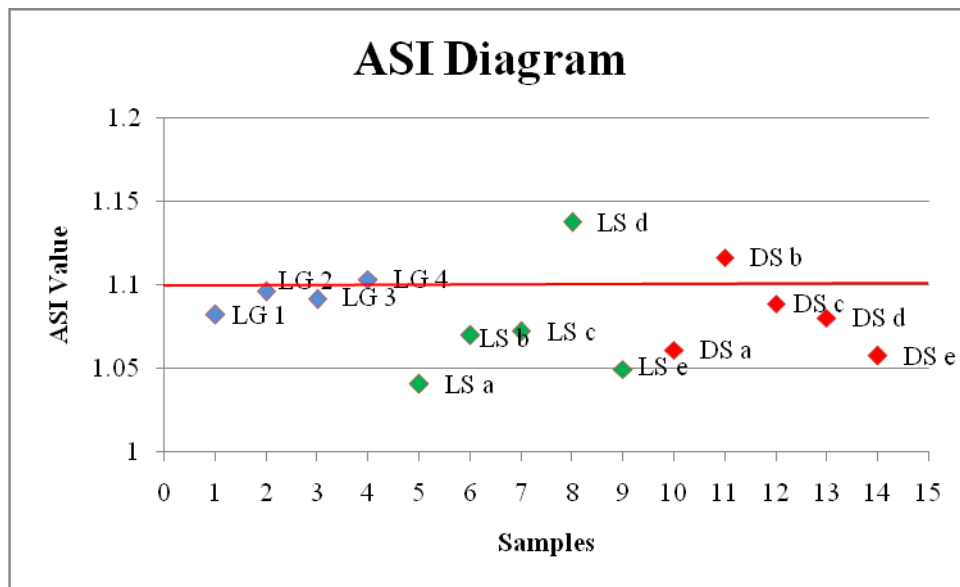


Figure 6.2, Aluminium Saturation Index (ASI) values for 4 leucogranite (LG) samples, 5 leucocratic megacrystic Stinkbank granite samples (LS) and 5 biotite-rich megacrystic Stinkbank granite samples (DS). The values for the leucogranites plot mostly above 1.1 and the biotite megacrystic Stinkbank granite values plot mostly below the 1.1 value.

Chappell and White (1974) noted that the Na₂O content of I- and S-type granites are relatively high (>3.2wt %) and low (<3.2wt %), respectively. Most of the biotite-rich and leucocratic megacrystic Stinkbank granite show Na₂O values > 3.2wt%, whereas the leucogranite shows consistently lower values of < 2.9wt%. Plotted on a Na₂O vs. K₂O diagram, Chappell and White (1974) constructed a line that supposedly divides a field of S- from I-type granites below and above this line, respectively (Figure 6.3). Samples of the Stinkbank granite describe a clear trend in this diagram. The leucogranites plot below the line, whereas the biotite-rich Salem-type granites plot above this line and into the field of I-type granites. The leucocratic megacrystic granite plots across the line and between the two end-member varieties of the Stinkbank granite.

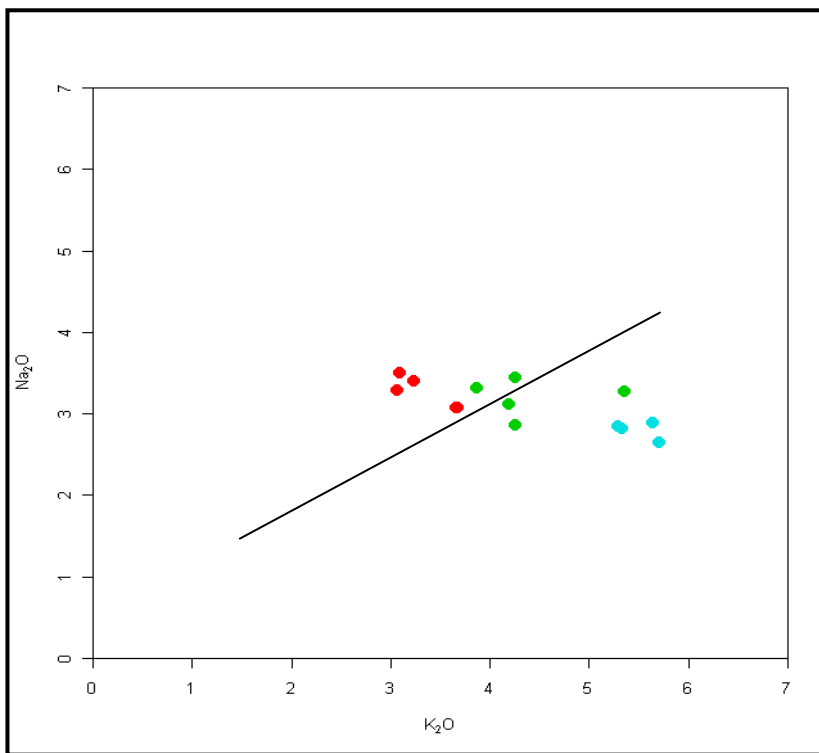


Figure 6.3, Na₂O vs. K₂O diagram, Chappell and White (1974) constructed a line that divides a field of S- from I-type granites. Samples of the Stinkbank granite describe a clear trend in this diagram. The leucogranites plot below the line, whereas the biotite-rich Salem-type granites plot above this line. The leucocratic megacrystic granite plots across the line and between the two end-member varieties of the Stinkbank granite.

In summary, based on geochemistry only, a clear distinction between S- and I-type origins for the different phases of the Stinkbank granites remains ambiguous. Geochemically, the biotite-rich megacrystic granite and the leucogranite are most distinct, whereas the leucocratic megacrystic granites seem intermediate between the two, sharing characteristics of both phases. A discussion of the geochemical results combined with petrographic findings for the granite phases will be presented in Chapter 7.

7. DISCUSSION

7.1. Regional strains

Wall-rock strains in rocks of the Kransberg syncline record a bulk co-axial NW-SE-directed subhorizontal shortening strain, evidenced by the upright to NW-verging folding (F_2) and foliation development (S_2) (e.g. Miller, 1983, 2008; Coward, 1983; Kasch, 1983). The structural imbrication of rocks of the Etusis with the Karibib Formation (Figure 3.3, c) and associated juxtaposition of basement and older Nosib Group rocks on top of the youngest formations of the Damara Supergroup also indicate the continuation of the regional-scale Mon Repos Thrust Zone (MRTZ). All this corresponds to D_2 crustal shortening strains that formed the main structural grain of the CZ and the Damara Belt as a whole.

The boudinage and folding of e.g. granite sills and dykes provide particularly sensitive strain gauges in the otherwise relatively homogeneous wall rocks of the mainly Kuiseb Formation. Shallowly-dipping boudin long axes in the immediate footwall of the MRTZ (Figure 4.12) agree with the regional NW-SE shortening and indicate a steep stretch, corresponding to the overall fold-and-thrust environment (i.e. horizontal shortening and vertical extension). For the most part, however, the chocolate-tablet boudinage suggests layer-normal shortening and no preferred or consistent direction of extension in the shortening plane (S_2). The D_2 tectonism occurred during peak-metamorphic conditions ($P = 3 \pm 1$ kbar, $T = 600\text{-}650^\circ\text{C}$), recorded by mineral assemblages that define regional fabrics and the predominantly ductile deformation of wall rocks. It is before this background that the emplacement of the Stinkbank granite has to be discussed.

7.2 Intrusive sequence and sheet-like geometry of the Stinkbank granite

Cross-cutting relationships outline a clear intrusive sequence in the main body of the Stinkbank granite from early biotite-rich megacrystic granites via leucocratic megacrystic granites to leucogranites (Chapter 5.3). This sequence of intrusion is a general feature of Salem-type granites (e.g. Jacob, 1974; Miller, 2008). The brecciation of older granite phases and/or wall rocks only occurs over a narrow, commonly less than 10m wide, gently undulating and folded surface. These contacts can be used to constrain the three-

dimensional geometry of individual granite phases and the granites thus delineated have the form of shallowly-dipping sheets, although subsequent folding has deformed the originally subhorizontal contacts (Figure 5.16 and 5.19)

Since both roof and floor rocks of individual sheets are only rarely exposed together, the actual thickness of the sheets is difficult to ascertain. In case of the biotite-rich megacrystic granite, the roof of the granite is indicated by the presence of abundant wall-rock xenoliths of the Kuiseb Formation. The lower contact is given by the occurrence of either the leucocratic megacrystic granite and/or where the granite has been brecciated by the leucogranite. This would correspond to a thickness of only ca. 20 m in the central parts of the Stinkbank granite, in the area around the Pramberg. (Figure 5.23, 5.24 and 5.25). In the north-central parts, the biotite-rich megacrystic granite has a thickness of at least 30 m, but outcrop is only sporadic here and upper and lower bounding surfaces can only be extrapolated between isolated pavements. Only the hanging-wall contact of the leucogranite is exposed, showing intrusive contacts either against the biotite-rich granite or wall rocks of the Kuiseb Formation in the SW termination of the Stinkbank granite. The minimum thickness of the leucogranite is 50 - 80 m, given the topographic relief around the Pramberg and in the main Khan River bed, but this must be speculative and the granite may be significantly thicker.

Taken in conjunction, the Stinkbank granite appears to be assembled by two main (biotite-rich megacrystic granite and leucogranite) and one subordinate (leucocratic megacrystic granite), stacked subhorizontal granite sheets that intruded sequentially. The brecciated contacts and angular xenoliths indicate that earlier sheets were crystallized before later sheets arrived at the emplacement site. Cross-cutting relationships and the position of granite phases with respect to each other also show that later phases intruded at and along the base of earlier granite phases. Overall, the intrusive relationships indicate that the Stinkbank granite seems to have been assembled from the top down, i.e. the magmatic accretion of younger sheets along the base of previously emplaced granite sheets. This also implies that the different granite pulses used similar emplacement paths, but that later magma pulses did not cross-cut earlier granite sheets. This would account for the well preserved pseudostratigraphy in the central parts of the Stinkbank granite. However, the outcrop pattern clearly documents the intrusion of the more voluminous

leucogranites beyond the extent of the earlier biotite-rich megacrystic granites, forming almost exclusively the lateral contacts with the wall rocks along domains 1 and 2. The abundance of wall-rock xenoliths in the biotite-rich megacrystic granite and its structural position above the leucogranite suggest that the biotite-rich granite occupied the roof zone of the granite sheet.

The sheet-like geometry and shallow dips of the sheets and the Stinkbank granite as a whole can also explain the large areal extent of the granite. At the same time, the granite would combine much lower amounts of melt compared to steep-sided batholithic complexes as which Salem-type granites are commonly depicted on regional sections (e.g. *Smith, 1965*). The bottom contact of the Stinkbank granite is not exposed. However, given that the granite is largely confined to the lower thirds of the Kuiseb Formation, not extending below the underlying marbles of the Karibib Formation, the laterally extensive (ca. 30 x 20 km full extent) Stinkbank granite may only show a thickness of up to 250-300m and possibly as little as 100m. This corresponds to the more recent cross-sections constructed by *Miller (2008)*.

The commonly sharp and intrusive relationships document that the earlier granites are not merely roof phases of later granites that have formed through e.g. the assimilation of wall-rock schists or in-situ differentiation (e.g. *Jacob, 1974; Miller, 1983, 2008*). Indeed, both petrographic and geochemical results point to possibly very different sources of the two main granite types. Important accessory phases in the biotite-rich megacrystic granite are e.g. sphene and hornblende (*Miller, 2008*), although the latter was not identified in samples of the Stinkbank granite. These phases are typically associated with granites of I-type affinity (e.g. *Chappell and White, 2001*). The later leucogranite is the other compositional end-member of the Stinkbank granite and is a garnetiferous, peraluminous, two-mica, monazite-bearing granite with a rather S-type affinity. Although not treated in depth, petrographic and geochemical results point to significantly different sources of the granites. This certainly opens up new avenues for research, trying to explain the spatial and temporal association of these seemingly very different granites that, on a regional scale, commonly combine to form the typical Salem-type granite association.

7.3 Synkinematic timing of granite plutonism and deformation of the Stinkbank granite.

The emplacement of Salem-type granites is commonly considered to have been syn- to post tectonic (D_2). In the sCZ, this is particularly true for the biotite-rich, megacrystic varieties, but Miller (2008) also cites the leucogranite variety of the Stinkbank granite as an example of a post-tectonic Salem-type granite.

The Stinkbank granite and related phases display overwhelming evidence for a syn- D_2 timing of emplacement, expressed by the (a) the formation of magmatic and solid-state fabrics in the granites (Figure 5.11, 5.12 and 5.13), (b) the folding of granite sheets (Figure 5.9 and 5.10), and (c) the deformation of sheet-like pegmatite and granite dykes related to the main Stinkbank granite in wall rocks (discussed under wall-rock strains, Chapter 7.1). It is only late-stage pegmatite and aplite dykes in the wall rocks and the main granite body that appear undeformed and posttectonic.

Magmatic and/or solid-state foliations are developed in all of the main phases of the Stinkbank granite (Figure 5.15). Throughout the granite, the foliation trends NE-SW and, thus, parallel to the regionally developed D_2 fabrics. This suggests that the fabric was not attained during e.g. magmatic flow, but that fabric formation tracks the regional strain field and crystallization of the granite during D_2 . The biotite-rich megacrystic granite shows stronger fabric intensities compared to e.g. the leucogranite, corresponding to the relative timing of the two and the accumulation of higher finite strains in the older granite compared to the younger intrusive. Foliation development is also stronger where the granites border against the steep, and isoclinally-folded and transposed wall rocks of domain 1, and fabric intensities in the wall rocks are clearly mimicked by those in the granites. Rotated magmatic and solid-state fabrics in xenoliths of the biotite-rich granite in leucogranites (Figure 5.18) are an important indicator of the fact that fabric development occurred during the emplacement of the various granite phases and that regional strains were not merely superimposed at a later stage.

Folding of the granite sheets of the Stinkbank granite is identified through the mapping of internal contacts between the main granite phases that are defined by the presence of intrusive breccias zones and/or wall-rock screens. Folds show NE trends and are

approximately upright and, thus parallel to the F_2 folds of wall rocks. Both magmatic and solid-state fabrics in the granites show an axial planar orientation with regard to the folds, underlining the origin of folding during regional shortening (D_2). All mapped folds are antiforms. Intervening synforms are likely to be present between antiforms, but their expression in the field is more subtle and the lack of mapable synforms is interpreted to be an artefact of exposure conditions rather than indicating an absence of synformal structures. The smaller antiforms are gently doubly plunging (NW-SE). However, the most prominent fold underlying the central Pramberg structure shows an overturned SW hinge, giving it an almost sheath-like geometry with a SW facing closure (Figure 5.19). The SW vergence and overturned geometry is a characteristic feature of regional-scale dome structures in this part of the sCZ. It is recorded in e.g. the Vergenoeg and Namibfontein domes to the immediate SW of the Stinkbank granite (*Kröner, 1984; Poli and Oliver, 2001; Figure 2.2*) and in the immediately adjacent Usakos dome to the SE (*Johnson, 2005; Johnson et al., 2006*). The resulting large-scale (>5-10km amplitude and wavelength) sheath folds are interpreted to indicate the orogen-parallel, SW directed extrusion and stretch of the orogen, normal to the main D_2 NW-SE directed collision (*Kisters et al., 2004*). Fold geometries in the granite are, thus, near-identical to regional-scale fold geometries developed in the surrounding wall rocks, underlining the syn- D_2 timing of granite emplacement.

7.4 The Stinkbank granite as a laccolith

The Stinkbank granite is overall ovoid in plan view. Its long axis trends NE-SW, parallel to the regional structural grain. The SW termination shows a characteristically lobate shape, with the wall rocks paraconformably wrapping around the granite contact. On a regional scale, wall-rock contacts are also conformable. Discordant contacts are only evident in the contact zones on a scale of meters or tens of meters and in the N parts of the SW termination, where the granites seemingly truncate a synclinal wall-rock structure at high angles. This area is largely overlain by younger cover and not well exposed.

The most noteworthy aspects that emerged during the mapping of the SW termination of the granite are (a) the closure of the Kransberg syncline as an antiform, showing paraconformable contacts with the underlying granite, and (b) the interference of folds, in

particular, the fact that the antiformal synclinal closure is all around rimmed by synformal structures. Interference between these synforms causes the formation of the characteristic bedding-triple junctions.

Two possible scenarios can be discussed.

(1) The antiformal fold closure in the hinge of the Kransberg syncline may represent a second-order fold and the antiform was intruded by the Stinkbank granite. Indeed, the preferential emplacement of granites in the hinge of particularly antiformal structures is a common feature of many plutons in the Damara Belt (*e.g. Miller, 1983; Johnson, 2005; Kisters et al., 2009*).

(2) The antiformal shape may reflect granite- and emplacement induced wall-rock strains. Many granites can be shown to have laccolithic or lopolithic geometries (*e.g. Pollard and Johnson, 1973; Cruden, 1998; Morgan et al. 2005, 2008*) in which the emplacement of the granite causes the roofs of the pluton to be uplifted and arched above the progressively inflating granite.

The steep, but conformable wall-rock contacts of the leucogranite, combined with the shallowly-dipping and folded internal contacts indicate that the granites have been affected by the regional D_2 folding (Chapter 5). Roof uplift in shallow-crustal laccoliths can be identified by strains in the wall rocks, *e.g.* indicating the stretching of the country-rocks above the granite, or *e.g.* contact-parallel fabrics in the granites, that would point to a contact-parallel flow of the melt (*e.g. Horsman et al., 2005*). In case of the Stinkbank granite, the identification of such strains is not possible because of the near-pervasive regional D_2 strains. However, the fold interference pattern of domain 2 provides possible clues. If the antiformal fold closure of the first-order Kransberg syncline was merely a second-order F_2 fold, fold trends would be expected to be NE-SW, parallel to the regional structural grain of F_2 folds (and thrusts). The high-angle refolding of the rim synforms (*e.g.* the Safier synform) around the SW termination of the Stinkbank granite and the resulting fold interference pattern do not agree with a simple F_2 fold pattern. Instead, the refolding and formation of bedding triple junctions rather suggest the superimposition of emplacement-related strains (roof uplift) onto regional strains (D_2 shortening). It also seems likely that the emplacement of the massive and, compared to the wall rocks

lithologies, relatively competent granite sheet has influenced further fold amplification during progressive shortening (D_2). In summary, it is suggested that the antiformal fold closure and paraconformable granite contacts as well as the fold-interference pattern in wall rocks in the SW termination of the Stinkbank granite probably reflect an initial roof doming of the wall rocks above the granite sheets, that was further amplified by regional F_2 folding. Together with the mainly concordant wall-rock contacts, this may point to the laccolithic geometry of this part of the Stinkbank granite. Given that the floor rocks are not exposed, lopolithic geometry could also be invoked.

7.5 The role of granite sheeting for the assembly of the Stinkbank granite

The two main and one minor, compositionally distinct phases seem to outline an internally sheeted nature of the Stinkbank granite. Sheets are largely concordant to each other and the wall-rocks. It is only the leucogranite that, in places shows internal layering and/or sheeting, parallel to the internal contacts between different phases (Figure 5.27). Despite this, the main phases seem internally relatively homogeneous, preserving little evidence of sheeting and/or multiple intrusive relationships. This would imply that the Stinkbank granite was assembled through only three main and compositionally distinct magma pulses. Possible evidence of internal granite sheeting is provided by the presence of the fine- to medium-grained magmatic enclaves in the leucogranite in the SW termination of the Stinkbank granite (Figure 5.26, a and b). Both the occurrence and orientation of enclaves are subparallel to the granite wall-rock contact. Provided that these granite enclaves also behaved as screens between different intrusive sheets, similarly to e.g., the breccia zones between the biotite-rich granite and leucogranite, the fragments would indicate the presence of at least two distinct leucogranite sheets, but this must remain tentative.

The internal homogeneity of the granite contrasts markedly with the multiple and sequential intrusive relationships that are well preserved along the margins and in the immediate wall-rocks of e.g. the leucogranite all along domains 1 and 2. The wall rocks are structurally overlying the main leucogranite and, thus, correspond to the roof of the Stinkbank granite. Cross-cutting relationships between sills and variable degrees of deformation document that granite sheeting occurred over a protracted period of time. In

sections along the Khan River, dozens and, probably, hundreds of sills and, thus, sheeting events can be identified (Figure 5.5). Granite sheeting is also indicated by the presence of wedge-shaped apophyses in the roof of the leucogranite in the SW termination of the leucogranite. Moreover, the incorporation of wall-rock xenoliths and stoping described in Chapter 5.3.4 along the SE granite contact against rocks of domain 1 clearly illustrates multiple sheeting and the sequential emplacement of granite sheets along the granite contact.

A relatively homogeneous interior of granites surrounded by sheeted margins is a commonly observed feature in many granite plutons worldwide (*e.g. Mahan et al., 2003; Johnson et al., 2003; Coleman et al., 2004; Belcher and Kisters, 2006*). In most of these cases, original sheeting in the pluton interior is thought to have been obliterated by a textural and compositional homogenization in a steady-state magma chamber that was created through progressive granite sheeting (*e.g. Yoshinobu et al., 1998; Glazner et al., 2004*). Granite sheets on the margins of the plutons are, in contrast, preserved as a result of the faster cooling of the individual sheets that may thereby retain their original textural and compositional characteristics. In the case of the Stinkbank granite, it is conceivable that high ambient wall-rock temperatures (ca. 600°C) during emplacement have facilitated the formation of steady-state magma chambers. The commonly only dm- to m-wide sills in the wall rocks that were evidently intruded over a protracted period of time underwent relatively fast cooling. The sum of the observations presented above suggests that a similar process can be invoked here for the Stinkbank granite, but field evidence for these processes is equivocal as is with most granite plutons (*e.g. Glazner et al., 2004*).

The predominance of sills illustrates the importance of the pre-existing bedding and/or foliation anisotropy for sheet propagation and emplacement. The vast majority of sills and dykes in the wall rocks show compositional similarities to the late-stage leucogranites in the main body of the Stinkbank granite. Most of these sills and subordinate dykes seem to have been emplaced when the rocks had attained steep attitudes, i.e. at a relatively late stage and when regional fold geometries were well established. This implies an emplacement of the mainly sills at high angles or normal to the principal shortening direction. Evidence for this is provided by the mainly-chocolate-tablet type boudinage experienced by many sills. The emplacement of sheet-like granites

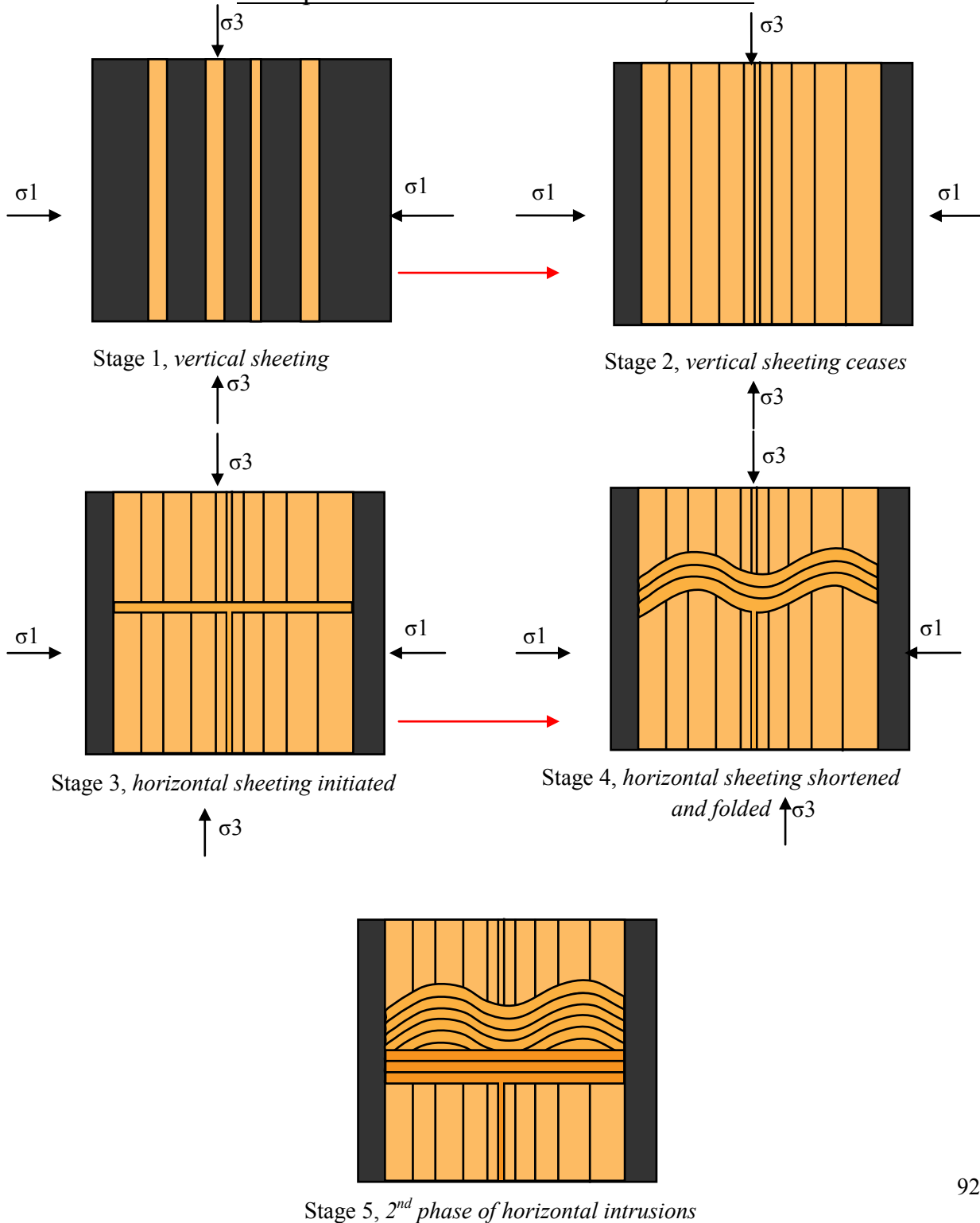
into the plane of shortening has been described from particularly mid- and lower crustal terrains where differential stresses are low (*e.g. Lucas and St. Onge, 1995; Brown, 2007; Kisters et al., 2009*). It indicates that the difference in tensile strength parallel and perpendicular to the plane of anisotropy is larger than the differential stress. Under these conditions sheets may intrude irrespective of the regional stress field, guided by the orientation of the pre-existing bedding anisotropies. The presence of refolded, originally boudinaged dykes (Figure 4.17) points to earlier sheet emplacement and prior to the final steepening of wall rock fabrics.

This relationship between sheet orientation, regional strains or principal stresses and the presence and/or absence of pre-existing anisotropies is particularly well illustrated for small-scale (100-150 m in diameter) granite stocks in wall-rock domain 1, shown in Figure 5.9. In this outcrop, a number of successively emplaced, distinct sheet geometries can be distinguished (Figure 5.10) describing a succession of sheet intrusions schematically shown in Figure 7.1

The earliest leucogranites intruded as vertical, bedding-parallel sills (Stage 1, Figure 7.). The presence of the bedding anisotropy controls the emplacement of the sheets, at high angles to the principal compressive stress. In places, the sills are texturally and also compositionally distinct and sheet-in-sheet contacts can be identified. This leads to the amalgamation of granite and pegmatite sheets to form a more massive granite (Stage 2, Figure 7.1) thereby obliterating the bedding anisotropy of the Kuiseb Formation. The amalgamated vertical sheets are truncated by high-angle granite and pegmatite sheets. This transition from bedding-parallel vertical sheeting to subhorizontal sheeting is interpreted to be in response to the mechanical homogenization formed by the amalgamation of earlier sheets. At this stage (Stage 3, Figure 7.1), the regional D_2 strains and stress field determine the orientation of sheets, favouring the emplacement of subhorizontal granite dykes. With progressive deformation, these shallowly-dipping sheets are folded into upright, NE-trending (F_2) folds (Stage 4, Figure 7.1). Still later dykes intrude as subhorizontal, cross-cutting sheets (Stage 5, Figure 7.1). The sheets remain planar and undeformed, pointing to their late-tectonic timing, i.e. in the presence of a regional stress field, but during the waning stages of deformation.

These intrusive relationships highlight the role of pre-existing anisotropies and, in particular, bedding for the emplacement of the granite sheets. This applies for the relatively thin granite sheets in the wall rocks, but is equally true for the emplacement of the main phases of the largely bedding/foliation concordant granite phases of the Stinkbank granite.

Multiple sheet intrusion mechanism, Model



7.6 Emplacement of the Stinkbank granite – towards an overall model

The previous chapters discussed the overall geometry of granite phases, internal and wall-rock contacts, progressive deformation and regional strains as well as granite sheeting associated with the Stinkbank granite. Based on this, the following chapter attempts to present an evolutionary sequence for the emplacement of the granite and related phases, summarized in Figure 7.2

Stage 1 (Figure 7.2, a)

The onset of regional deformation, D_2 , is accompanied by the intrusion of the first granite, the biotite-rich megacrystic Stinkbank granite. The present, subhorizontal and largely concordant geometry suggest that the granite intruded into still subhorizontal bedding of the Kuiseb Formation, early D_2 . A possibly disc- or wedge- shaped geometry is indicated by a thickening of the megacrystic granite towards the NE. Brecciation of the wall rocks is common along an up to 5-10m wide zone, particularly along the top of the granite. Magmatic and progressively solid-state, NE-SW trending foliations are formed during and following crystallization of the granite. There are no granite sheets with similar compositions to that of the megacrystic granite in the wall rocks so that the feeder to the earliest granites of the Stinkbank granite remains elusive (here schematically shown as a vertical feeder).

Stage 2 (Figure 7.2, b)

The start of stage 2 is characterized by the intrusion of the first leucogranite sheets, mainly in the form of bedding parallel sills. The sills make use pre-existing bedding anisotropies as fracture pathways. Subhorizontal shortening (D_2) is accommodated by the wall-rocks in the form of large open folds. The regional shortening causes the development of a S_2 , NE-SW trending, subvertical foliation.

Stage 3 (Figure 7.2, c)

During progressive shortening (D_2), wall-rock structures are tightened and amplified. The tightening of F_2 folds is pronounced in the wall-rocks, whereas the 20-30 m thick, competent biotite-rich megacrystic granite delays fold amplification. Earlier leucogranite sills become boudinaged, if they intruded vertically, and folded if they intruded in a subhorizontal fashion.

Stage 4 (Figure 7.2, d)

With further shortening, earlier steep sills undergo chocolate tablet boudinage, whereas cross-cutting shallowly-dipping dykes are folded. Granite sheeting continues in the wall rocks. During this stage (syn- to late D₂) the main leucogranite intrudes beyond the original confines of the original megacrystic granite. Inflation of the leucogranite is interpreted to have caused the uplift of roof rocks, which was then amplified during progressive shortening, resulting in the antiformal synclinal structure in the SW of the Stinkbank granite and interference folding in domain 2. Progressive shortening caused the folding of the originally shallowly-dipping intrusive contacts between the granite phases and late-stage, SW verging overfolding (not shown here) corresponds to the lateral, orogen-parallel extrusion of the rocks (*e.g. Coward, 1983; Kisters et al., 2004*). The S₂ foliation (solid-state) still affected the last phases of the Stinkbank granite. Truly post-tectonic intrusive are only expressed by cross-cutting pegmatite dykes in the wall rocks.

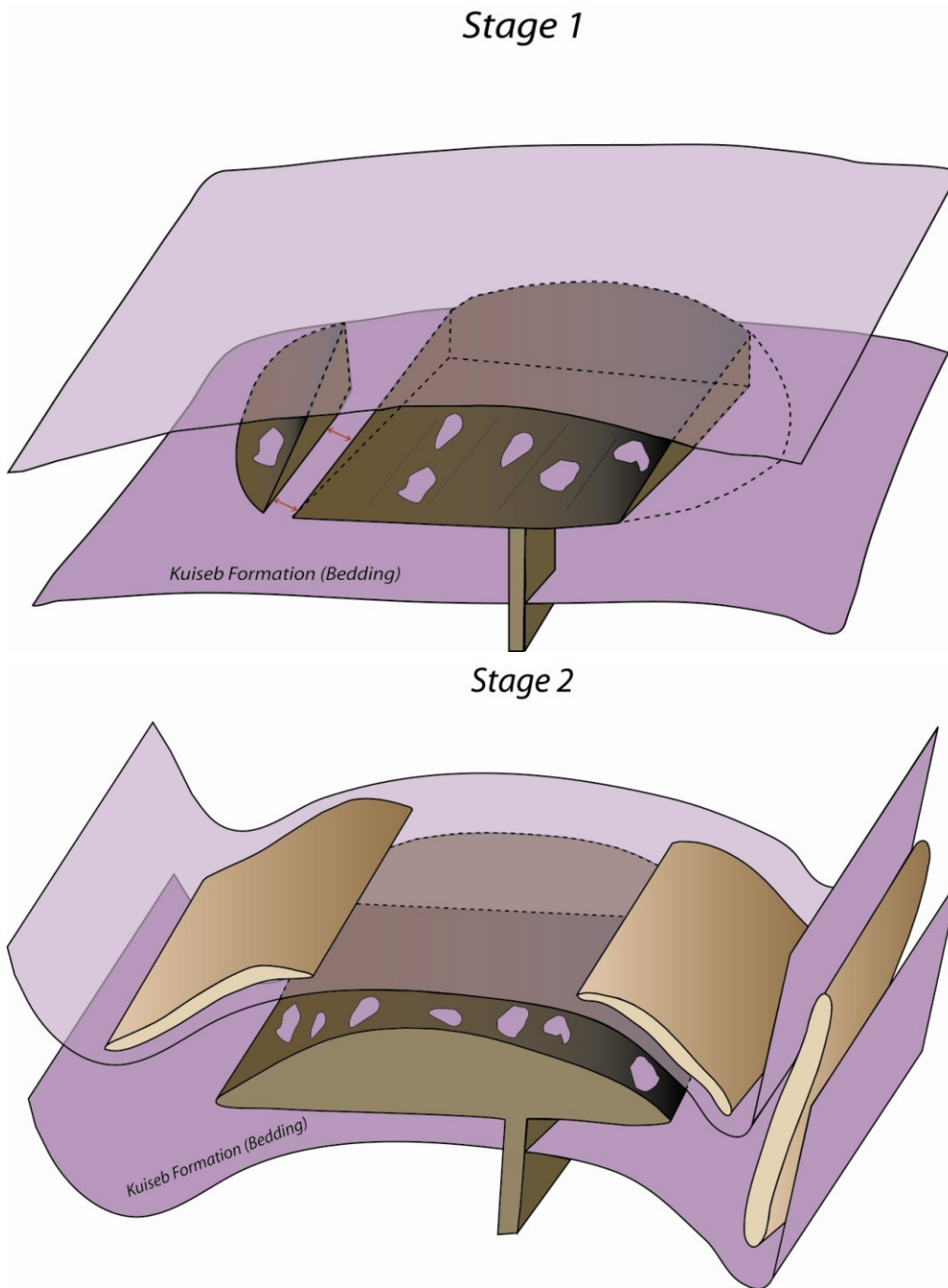


Figure 7.2 a), emplacement of the early biotite-rich, megacrystic Stinkbank granite during early D_2 . The presents outcrop suggests a probably arc- or wedge- shaped geometry (cut open here to show the lateral thickness variations) b) Emplacement of leucogranite sheets in wall rocks during D_2 . The granite sheets are likely to be precursor phases to the main leucogranite body. See text for detailed explanation.

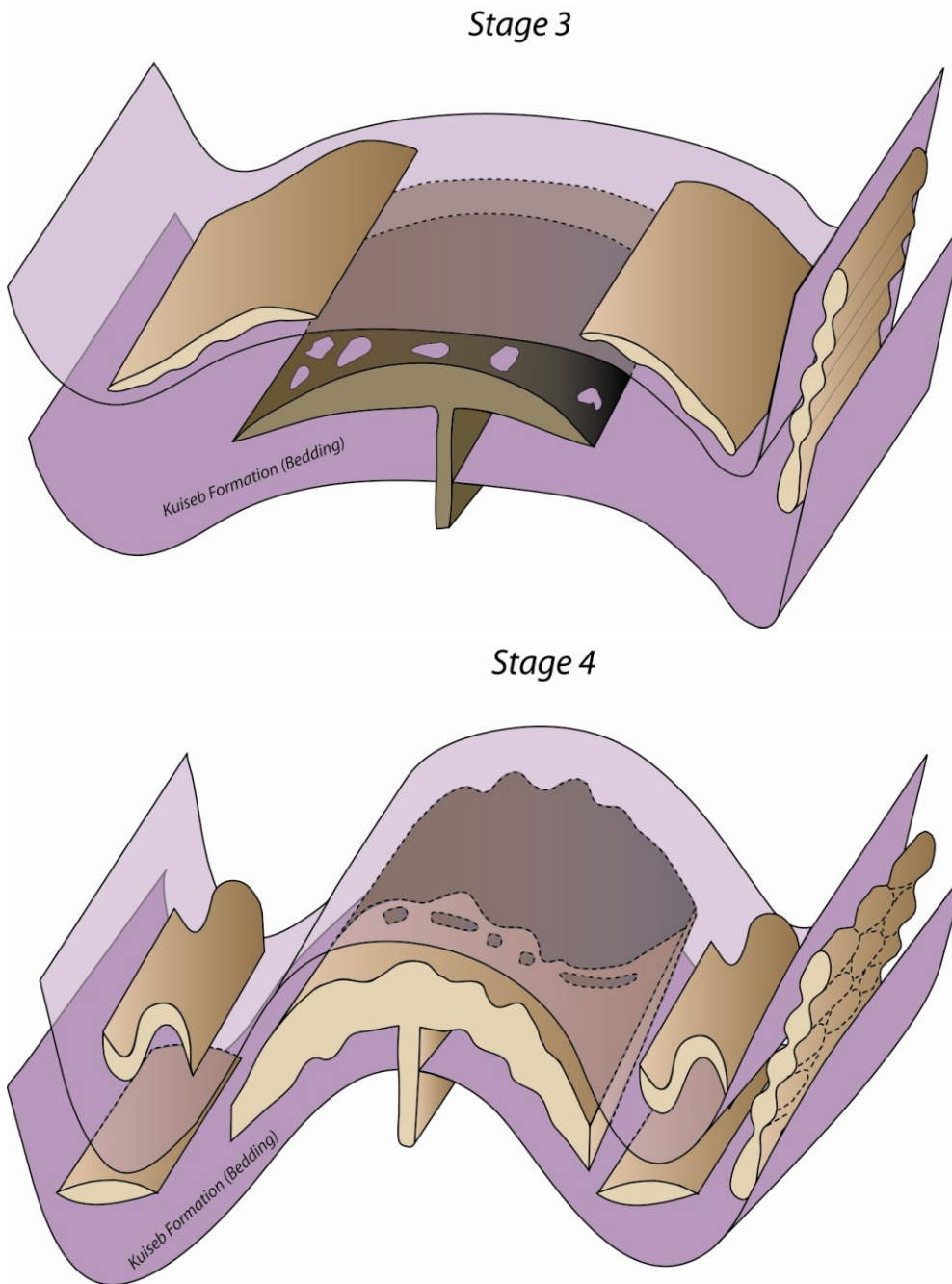


Figure 7.2 c) Progressive D₂ shortening and deformation of earlier intrusive phases. d) Emplacement and deformation of the main leucogranite, folding of internal granite contacts, deformation of earlier granite sheets in wall rocks and emplacement of late-stage, discordant sheets. See text for detailed explanation.

7.7 Regional controls of emplacement

The regional controls of emplacement of Salem-type granites in predominantly synformal structures, in the basal portions of the Kuiseb Formation and above marbles of the Karibib Formation (*e.g. Miller, 1983*) remain a somewhat enigmatic point. Numerous studies have shown that the ductilely deforming, thick (>500-1000m) marble sequences of the Karibib Formation effectively act as barriers for fracture propagation and melt transport (*e.g. Miller, 1983; Johnson et al., 2006; Kisters et al., 2009*). The tips of granite and pegmatite dykes blunt upon entering the marble units, commonly leading to a ponding of melts below the marbles. In fact, numerous small, and regional-scale granite plutons can be shown to pond below shallowly-dipping marble units, particularly in and below antiformal fold closures capped by marbles (*e.g. Miller, 1983*).

Around the Stinkbank granite in e.g. domain 1, the marbles of the Karibib Formation reach a thickness of, on average, only 20-100m. In contrast, the Karibib Formation is up to >1500m thick some 20-30km along strike to the NE. Here, no Salem-type granites are developed (*Johnson, 2005*). This thinning of the marbles is not due to primary facies variations, but rather structural in origin. It marks the presence of the Mon Repos Thrust Zone (Chapter 4). As such, the significantly thinner marble units at and around the emplacement site of the Stinkbank granite may have allowed for the penetration of granite sheets through the thin marble units. Thicker marbles may have arrested melt transport in fractures, the demonstrably most important mode of melt transport in this part of the Damara Belt. It has to be investigated on a regional scale whether this pattern of thinned marble units and presence of Salem-type granites can be confirmed.

The occurrence of Salem-type granites in predominantly synformal structures cored by the Kuiseb Formation may merely be an artefact of the preservation of the rocks. As the Kuiseb Formation forms the stratigraphically uppermost unit of the Damara Supergroup, the rocks are most commonly preserved in regional-scale synforms, or synclines. In any case, the early D₂ timing and bedding-parallel, sill-like geometry of the early phases of the Salem-type granites (the biotite-rich, megacrystic granite) highlights the role of shallowly-dipping anisotropies for granite emplacement. The interface between the Karibib and well-bedded Kuiseb Formation has most likely presented a prominent bedding anisotropy and rheological boundary that led to the arrest of early D₂ intrusives, i.e. before or at an early stage of fold amplification and steepening of wall

rocks. Hence, the close spatial association of Salem-type granites with synformal structures cored by Kuiseb schists may also reflect a temporal relationship, i.e. the presence of Salem-type melts during the early D₂ stage of deformation and fold amplification.

8. CONCLUSIONS

- The 600 km² Stinkbank granite forms part of the Salem-type group of granites. Detailed and regional mapping of the Stinkbank granite has shown that the pluton consists of an amalgamation of multiple, and three major, compositionally distinct granite sheets. These sheets are relatively thin, generally not more than a few tens of meters thick. The granite sheets are intrusive into wall rocks of the Kuiseb Formation in the core of the first-order NE-trending (D₂) Kransberg syncline.
- Intrusive contact relationships and petrographic and geochemical characteristics indicate that each of the three major granite phases represents a distinct emplacement pulse. Evidence for in-situ differentiation processes or wall-rock assimilation, commonly stated to account for the compositional variation of Salem-type granites, were not identified.
- The mainly concordant granite wall-rock contacts and internally concordant contacts between different granite phases indicate an overall sill-like, possibly laccolithic shape for the Stinkbank granite. The laccolith-like shape is evidenced in the closure of the Kransberg syncline in the SW, where the wall-rocks outline an antiformal shape that is interpreted to be inherited from the roof uplift of the intruding granite.
- The sequential emplacement of granite sheets, from early biotite-rich, megacrystic granites to late-stage leucogranites has created a pseudostratigraphy. Cross-cutting relationships indicate that the thin and planar Stinkbank granite was assembled from the top down and through the accretion of younger granite sheets at the base of earlier intrusive phases.
- Emplacement of the Stinkbank granites occurred early- to syn- D₂ and into initially horizontal strata. Granite emplacement occurred throughout the D₂ deformation as indicated by the progressive granite sheeting and deformation of intrusive sheets preserved in wall rocks. The major subhorizontal granite phases in the main body of the Stinkbank granite can be shown to be folded into NE-trending, upright doubly plunging

to, in places, overturned and sheath-fold like kilometre-scale folds. These folds are parallel to regional-scale F_2 folds in the wall rocks.

- NE-trending, magmatic and/or solid-state foliations are almost ubiquitous and developed in almost all granite phases. The foliation in the granite is largely axial planar to the folded granite sheets, underlining the syn- D_2 emplacement and progressive deformation of the Stinkbank granite.
- Granite sheeting and the progressive assembly of the Stinkbank granite through discrete, smaller magma batches is particularly well displayed by the multitude of cross-cutting and variably deformed granite sheets in the wall rocks and along the margins of the granite. A similar process of multiple granite sheeting is also assumed for the main, more homogeneous interior of the pluton, but textural and compositional evidence is less conclusive.
- The stratigraphic position of the Stinkbank granite in a regional scale syncline and at the base of the Kuiseb Formation is interpreted to reflect (a) the relatively early (D_2) timing of Salem-type granites, intruding into still subhorizontal country rocks before fold (F_2) amplification and steepening of the Damara Supergroup, (b) an emplacement along or immediately above a regionally important rheological interface (in siliciclastic units of the Kuiseb Formation and above the marble-dominated Karibib Formation), and (c) an intrusion through structurally thinned marbles that would otherwise inhibit fracture propagation. In general, the preservation of Salem-type granites in regional synforms may represent an artefact, given that rocks of the Kuiseb Formation, the uppermost succession of the Damara Supergroup, are mostly preserved in regional-scale synforms rather than antiforms.

9. REFERENCES

- Ameglio, L., Page, P., Jacob, R.E. (2000).** 3D-geometry of the Mon Repos granodiorite (Goas dioritic suite, Damara Belt, Namibia) inferred from gravity data. *Journal of African Earth Science* 31, p.2.
- Archanjo, C.J., da Silva, E.R. and Caby, R. (1999).** Magnetic fabric and pluton emplacement in a transpressive shear zone system: the Itaporanga porphyritic granitic pluton (northeast Brazil), *Tectonophysics* 312, 331–345
- Badenhorst, F.P. (1992).** The lithostratigraphy of area 2115B and D in the central zone of the Damara Orogen in Namibia: with emphasis on facies changes and correlation, unpublished thesis. University of Port Elizabeth, p. 124.
- Basson, I.J. and Greenway, G. (2004).** The Rössing Uranium Deposit: A product of late tectonic localization of uraniferous granites in the Central Zone of the Damara Orogen, Namibia. *Journal of African Earth Sciences* 38, 413-435.
- Belcher, R.W. and Kisters, A.F.M. (2006).** Progressive adjustments of ascent and emplacement controls during incremental construction of the 3.1 Ga Heerenveen batholith, South Africa. *Journal of Structural Geology* 28, 1406-1421
- Brown, M. (1994a).** The generation, segregation, ascent and emplacement of granite magma: the migmatite to crustally-derived granite connection in thickened orogens. *Earth Science Reviews* 36, 83–130.
- Brown, M. (1994b).** The generation, segregation, ascent and emplacement of granite magma: the migmatite-to-crustally-derived granite connection in thickened orogens. *Earth-Science Reviews* 36, 83–130.
- Brown, M (2007).** Crustal melting and melt extraction, ascent and emplacement in orogens: mechanisms and consequences. *Journal of the Geological Society*, v. 164; 709-730
- Brown, M. & Solar, G.S. (1998a).** Shear zone systems and melts: feedback relations and self-organization in orogenic belts. *Journal of Structural Geology* 20, 211–227.
- Brown, M. & Solar, G.S. (1998b).** Granite ascent and emplacement during contractional deformation in convergent orogens. *Journal of Structural Geology* 20, 1365–1393.
- Chappell, B.W. (1999).** Aluminium saturation in I- and S-type granites and the characterization of fractionated haplogranites. *Lithos* 46, 535–51.

- Chappell, B.W. and White, A.J.R. (1974).** Two contrasting granite types. *Pacific geology* 8, 173-174
- Chappell, B.W. and White, A.J.R. (2001).** Two contrasting granite types: 25 years later. *Australian Journal of Earth Sciences* 48, 489-499.
- Clemens, J.D. (2003).** S-type granitic magmas — petrogenetic issues, models and evidence. *Earth-Science Reviews* 61, 1–18.
- Clemens, J.D., and Mawer, C.K. (1992).** Granitic magma transport by fracture propagation. *Tectonophysics* 204, 339–360.
- Clemens, J.D. and Petford, N. (2000).** Granites are not diapiric! *Geology Today* 16 (5), 180-184
- Coward, M.P. (1983).** The tectonic history of the Damaran Belt. In: Miller, R.McG. (Ed), *Evolution of the Damara Orogen of South West Africa*. Special Publication of the Geological Society of South Africa 11, 409-421
- Cox, K.G., Bell, J.D. and Pankhurst, R.J. (1979).** *The Interpretation of Igneous Rocks*. George Allen and Unwin, London, 450 pp.
- Cruden, A.R. (1998).** On the emplacement of tabular granites. *Journal of the Geologic Society*, London 155, 853–862.
- De Kock, G.S., Eglington, B., Armstrong, R.A., Harmer, R.E. & Walraven, F. (2000).** U–Pb and Pb–Pb ages of the Naauwpoort rhyolite, Kawakeup leptite and Okongava Diorite: implications for the onset of rifting and of orogenesis in the Damara Belt, Namibia. *Communications of the Geological Survey of Namibia* 12, 81–88.
- Dixon, J.M. (1975).** Finite strain and progressive deformation in models of diapiric structures. *Tectonophysics* 28, 89–124.
- Foster, D.A., Goscombe, B., Passchier, C.W. and Trouw, R.A.J. (2006).** $^{40}\text{Ar}/^{39}\text{Ar}$ thermochronology of the Pan-African Damara Orogen, Namibia, with implications for tectonothermal and geodynamic evolution. *Precambrian Research* 150, 49-72
- Fowler, T.K. Jr. (1994).** Using geologic maps to constrain pluton emplacement mechanisms. *Geological Society of America, Abstracts with Program*. 26, 52.
- Fowler, T.K. Jr., Paterson, S.R., Crossland, A. and Yoshinobu, A. (1995).** Pluton emplacement mechanisms: A view from the roof. In: M. Brown and P.M. Piccoli, Editors, *The Origin of Granites and Related Rocks* US Geological Survey Circular 1129, 57.

- Glazner, A.F. and Bartley, J.M. (2006).** Is stopping a volumetrically significant pluton emplacement process? Geological Society of America Bulletin 118, 1185–1195.
- Glazner, A.F., Bartley, J.M., Coleman, D.S., Gray, W. and Taylor, R.Z. (2004).** Are plutons assembled over millions of years by amalgamation from small magma chambers? GSA Today 14, 4–11.
- Gray, D.R., Foster, D.A., Goscombe, B., Passchier, C.W. and Trouw, R.A.J. (2006).** $^{40}\text{Ar}/^{39}\text{Ar}$ thermochronology of the Pan-African Damara Orogen, Namibia, with implications for tectonothermal and geodynamic evolution. Precambrian Research, 150, 49–72.
- Hartnady, C., Joubert, P. and Stowe, C. (1985).** Proterozoic crustal evolution in southwestern Africa, Episodes 8, 236–244.
- Henry, G., Stanistreet, I.G. and Maiden, K.J. (1988).** Timing of continental breakup in the Damara Orogen: A review and discussion. Extended Abstracts. Geocongress 88, Geological Society of South Africa, Durban, 267-270
- Hoffmann, K.H. (1990)** Sedimentary depositional history of the Damara Belt related to continental breakup, passive margin to active margin transition and foreland basin development. Extended Abstracts. Geocongress 90, Geological Society of South Africa, Cape Town, 250-253
- Hoffman, P.F., Hawkins, D.P., Isachsen, C.E and Bowring, S.A (1996).** Precise U–Pb zircon ages for early Damaran magmatism in the Summa Mountains and Welwitschia Inlier, northern Damara Belt, Communications of the Geological Survey Namibia 11, 47–52
- Hoffmann, K.-H., Condon, D.J., Bowring, S.A. and Crowley, J.L. (2004).** U-Pb zircon date from the Neoproterozoic Ghaub Formation, Namibia: Constraints on Marinoan glaciation. Geology 32, 817-820.
- Horsman, E., Tikoff, B. and Morgan, S. (2005).** Emplacement-related fabric and multiple sheets in the Maiden Creek sill, Henry Mountains, Utah, USA, Journal of Structural Geology 27, 1426–1444.
- Horsman, E., Morgan, S., Stanik, A., Tikoff, B., de Saint Blanquat, M., Habert, G. (2008).** Emplacement of multiple magma sheets and wall rock deformation: Trachyte Mesa intrusion, Henry Mountains, Utah. Journal of Structural Geology, Volume 30, Issue 4491-512
- Hutton, D.H.W. (1988).** Granite emplacement mechanisms and tectonic controls: Inferences from deformation studies. Transactions of the Royal Society of Edinburgh, in press. Earth Sciences 79, 245–255.

- Jacob, R.E. (1974).** Geology and metamorphic petrology of part of the Damaran Orogen along the lower Swakop River, South West Africa. Bulletin of the Precambrian Research Unit, University of Cape Town 17, 201.
- Jacob, R.E., Snowden, P.A. and Bunting, F.J.L. (1983).** Geology and structural development of the Tumas Basement Dome and its cover rocks. In: Miller, R.McG. (Ed), Evolution of the Damara Orogen of South West Africa. Special Publication of the Geological Society of South Africa 11, 157-172
- Jacob, R.E., Moore, J.M., and Armstrong, R.A. (2000).** Zircon and titanite age determination from igneous rocks in the Karibib District, Namibia: implications for Navachab vein-style gold mineralization. Communications of the geological Survey Namibia 12, 157-166
- Johnson, S.D. (2005).** Structural geology of the Usakos dome, Damara Belt, central Namibia. Unpublished MSc thesis, University of Stellenbosch, p. 159.
- Johnson, S.D., Poujol, M, and Kisters, A.F.M. (2006a).** Constraining the timing and migration of collisional tectonics in the Damara Belt, Namibia: U-Pb zircon ages for the syntectonic Salem-type Stinkbank granite. South African Journal of Geology 109, 427-440
- Johnson, S.E., Gerbi, C. and Paterson, S.R. (2004).** Implications of rapid, dike-fed pluton growth for host-rock strain rates and emplacement mechanisms, Journal of Structural Geology 26, 583–594.
- Johnson, S.E., Fletcher, J.M., Fanning, C.M., Vernon, R.H., Paterson, S.R., Tate, M.C. (2003).** Structure, emplacement and in-situ expansion of the San Jose´ tonalite pluton, Peninsular Ranges batholith, Baja California, Mexico. Journal of Structural Geology 25, 1933-1957.
- Johnson, S. P., De Waele, B., Evans, D., Tembo, F. and Banda, W. (2006b).** A record of Neoproterozoic divergent processes along the southern Congo Craton margin. In: XXI Colloquium of African Geology, Abstract Book, Maputo, Mozambique, 73–74.
- Jung S. and Mezger, K. (2001).** Geochronology in migmatites - A Sm-Nd, U-Pb and Rb-Sr study from the Proterozoic Damara Belt (Namibia) and implications for polyphase development of migmatites in high-grade terranes. Journal of Metamorphic Geology 19, 77-79.
- Jung, S. and Mezger, K. (2003).** Petrology of basement-dominated terranes: I Regional metamorphic T-t path from U-Pb monazite and Sm-Nd garnet geochronology (Central Damara Orogen, Namibia). Chemical Geology 198, 223-247.

- Jung, S., Mezger, K. and Hoernes, K. (1998).** Petrology and geochemistry of syn- to post-collisional metaluminous A-type granites - a major and trace element and Nd-Sr-Pb-O-isotope study from the Proterozoic Damara Belt, Namibia. *Lithos* 45, 147-175
- Jung, S., Mezger, K. and Hoernes, S. (2001).** Trace element and isotopic (Sr, Nd, Pb, O) arguments for a mid-crustal origin of Pan-African garnet-bearing S-type granites from the Damara orogen (Namibia). *Precambrian Research* 110, 325–355.
- Kasch, K.W. (1983).** Continental collision, suture progradation and thermal relaxation: a plate tectonic model for the Damara orogen in central Namibia. In: Miller, R. McG. (Ed.), *Evolution of the Damara Orogen of South West Africa/Namibia*. Geological Society of South Africa Special Publication 11, 423–429.
- Kisters A.F.M., Ward, R.A., Anthonissen, C.J. and Vietze, M.E. (2009).** Melt segregation and far-field melt transfer in the mid-crust. *Journal of the Geological Society* 166, 905-918.
- Kisters, A.F.M., Jordaan, L.S. and Neumaier, K. (2004).** Thrust-related dome structures in the Karibib district and the origin of orthogonal fabric domains in the south Central Zone of the pan-African Damara Belt, Namibia. *Precambrian Research* 133, 283-303.
- Kitt, S. (2008).** Structural controls of auriferous quartz veins in the Karibib area, southern central zone of the pan-African Damara Belt, Namibia. unpublished MSc. thesis. University of Stellenbosch, 110.
- Kröner, A. (1982).** Rb/Sr geochronology and tectonic evolution of the Pan- African Damara Belt of Namibia, Southwestern Africa, *American Journal of Science* 282, 1471-1507.
- Kröner, A. (1984).** Dome structures and basement reactivation in the Pan-African Damara Belt of Namibia/South West Africa. In: Kröner, A., Greiling, R.O. (Eds.), *Precambrian Tectonics Illustrated*. Naegle and Obermiller, Stuttgart, Germany, pp. 191–206.
- Kukla, C., Kramm, U., Kukla, P.A. and Okrusch, M. (1991).** U-Pb monazite data relating to metamorphism and granite intrusion in the northwestern Khomas Trough, Damara Orogen, Central Namibia: *Communications of the Geological Survey Namibia* 7, 49–54.
- Lucas, S.B., and St-Onge, M.R. (1995).** Syn-tectonic magmatism and the development of compositional layering, Ungava Orogen (northern Quebec, Canada). *Journal of Structural Geology* 17, 475-491.
- Mahan, K.H., Bartley, J.M., Coleman, D.S., Glazner, A.F. and Carl, B.S. (2003).** Sheeted intrusion of the synkinematic McDoogle pluton, Sierra Nevada, California. *Geological Society of America Bulletin* 115, 1570-1582.

- Marlow, A.G. (1983).** Geology and Rb-Sr geochronology of mineralised and radioactive granites and alaskites, Namibia. Special Publications Geological Society of South Africa, II, 289-248
- Martin, H. (1965).** The Precambrian geology of South West Africa and Namaqualand. Precambrian Research Unit Bulletin, University of Cape Town, 159 pp.
- Masberg, P., Hoffer, E. and Hoernes, S. (1992).** Microfabrics indicating granulite-facies metamorphism in the low-pressure central Damara Orogen, Namibia. Precambrian research 55, 243-257.
- McCaffrey, R. (1992).** Oblique plate convergence, slip vectors, and forearc deformation, Journal of Geophysical Research 97, 8905-8915.
- McCaffrey, K.J.W. and Petford, N. (1997).** Are granitic intrusions scale invariant? Journal Geological Society, London 154, 1-4.
- McLaren, A.C. and Pryer, L.L. (2001).** Microstructural investigation of the interaction and interdependence of cataclastic and plastic mechanisms in feldspar crystals deformed in the semi-brittle field. In: Boland, J., Ord, A. (Eds.), Deformation Processes in the Earth's Crust. Tectonophysics 335, 1-15.
- Miller, R.B. and Paterson, S.R. (1994).** The transition from magmatic to high-temperature solid-state deformation: implications from the Mount Stuart Batholith, Washington. Journal of Structural Geology 16, 853-865.
- Miller, R. McG. (1983).** The Pan-African Damara Orogen of South West Africa/ Namibia. In: Miller, R.McG. (Ed.), Evolution of the Damara Orogen of South West Africa. Geological Society of South Africa, Special Publication, 11, 431-515
- Miller, R. McG. (1988).** Geological Map of the Damara Orogen, South West Africa/ Namibia. Geological Survey, Windhoek.
- Miller, R. McG. (2008).** The Geology of Namibia, Neoproterozoic to lower paleozoic, Volume 2, 13-357 – 13-372
- Miller, R.McG, Barnes, S. and Balkwill, G. (1983)** Possible active margin deposits within the southern Damara orogen: The Kuiseb Formation between Okahandja and Windhoek. In: Miller, R.McG. (Ed.), Evolution of the Damara Orogen of South West Africa. Geological Society of South Africa, Special Publication 11, 73-88
- Nash, C.R. (1971).** Metamorphic petrology of the SJ area, Swakopmund District, Namibia. Bull. Chamber Min. Precambrian Research Unit Bulletin, Univ. Cape Town, 9, 77 p.
- Oliver, G.J.H. (1994)** Mid-crustal detachment and domes in the central zone of the Damaran orogen Namibia. Journal of African Earth Sciences 19, 331-344.

- Paterson, S.R. and Fowler, T.K. Jr (1993).** Re-examining pluton emplacement processes. *Journal of Structural Geology*, 15, 191–206.
- Paterson, S.R., Vernon, R.H. and Tobisch, O.T. (1989).** A review of criteria for the identification of magmatic and tectonic foliations in granitoids. *Journal of Structural Geology* 11, 349–363.
- Parsons, T., Sleep, N.H and Thompson, G.H. (1992).** Host rock rheology controls on the emplacement of tabular intrusions: implications for underplating of extending crust. *Tectonics* 11, 1348–1356.
- Petford, N., Cruden, A.R., McCaffrey, K.J.W. and Vigneresse J.L. (2000).** Granite magma formation, transport and emplacement in the Earth's crust. *Nature* 408, 669–673.
- Pitcher, W.S. (1979).** The Nature, Ascent and Emplacement of Granitic Magmas, *Journal of the Geological Society of London*, 136, 627-662.
- Pitcher, W.S. (1997).** The nature and origin of granite, 2nd edn. Chapman and Hall, New York, p 387.
- Pollard, D.D. and Johnson, A.M. (1973).** Mechanics of growth of some laccolith intrusions in the Henry mountains, Utah, II; bending and failure of overburden layers and sill formation. *Tectonophysics* 18, 311-354.
- Poli, L. and Oliver, G.J.H. (2001).** Constrictional deformation in the Central Zone of the Damara orogen, Namibia, *Journal of African Earth Sciences* 33, 303-321
- Porada, H. (1989),** Pan African rifting and orogenesis in southern to equatorial Africa and eastern Brazil, *Precambrian Research* 44, 103–136.
- Puhan, D. (1983).** Temperature and pressure of metamorphism in the central Damara orogen. In: Miller, R. McG. (Ed.), *Evolution of the Damara Orogen of South West Africa/Namibia*. Geological Society of South Africa, Special Publication, 219–223.
- Ramsay, J.G. (1989).** Emplacement kinematics of a granite diapir: The Chindamora batholith, *Zimbabwe Journal of Structural Geology* 11, 191–209
- SACS, South Africa Committee for Stratigraphy (1980).** Stratigraphy of South Africa. Kent, L.E. (comp); Part 1. Lithostratigraphy of the Republic of South Africa, South West Africa/Namibia, and the Republics of Bophuthatswana, Transkei and Venda. Handbook geological Survey of South Africa, 8, 690 pp.
- Sawyer, E.W. (1976).** The geology of an area south east of Walvis Bay. Part 1: Lithology, sedimentation and field relationships. Open File Report of the geological Survey Namibia, RG 3, 136 pp.

- Smith, D.A.M. (1965).** The geology of the area around the Khan and Swakop rivers in South West Africa. Mem. Geologic Survey of South Africa, South West Africa Series, 3, 113pp.
- Stanistreet et al. (1991).** Sedimentary basinal responses to a Late Precambrian Wilson Cycle: the Damara Orogen and Nama Foreland, Namibia. *Journal of African Earth Sciences*, 13, 1141-156
- Steven, N.M. (1993).** A study of epigenetic mineralization in the Central Zone of the Damara Orogen, Namibia, with special reference to gold, tungsten, tin and rare earth elements. *Memoir Geol. Survey Namibia*, vol. 16, p. 166.
- Tack, L. and P. Bowden (1999).** Post-collisional granite magmatism in the central Damara (Pan-African) Orogenic belt western Namibia, *Journal of African Earth Science* 28, 653–674.
- Tack, L., Williams, I. and Bowden, P. (2002).** SHRIMP constraints on early post collisional granitoids of the Ida dome, central Damara (Pan African) Belt, western Namibia. Abs. 11th IAGOD Quadrennial Symposium & Geocongress, Windhoek, Namibia. Geological Survey Namibia
- Taylor, St.R. and McLennan, S.M., (1985).** *The Continental Crust: its Composition and Evolution.* Blackwell Scientific Publications: Oxford, 312 pp.
- Vernon, R.H. (2000)** Review of microstructural evidence of magmatic and solid-state flow. *Electronic Geosciences* 5:2.
- Vernon, R.H. (2004)** *A Practical Guide to Rock Microstructure.* Cambridge University Press, Cambridge. 610 pp.
- Vigneresse, J.L. (1995).** Control of granite emplacement by regional deformation. *Tectonophysics* 249, 173–86.
- Vigneresse J.L. and Clemens, J.D. (2000).** Granitic magma ascent and emplacement: neither diapirism nor neutral buoyancy. In: B. Vendeville, Y. Mart and J.L. Vigneresse, Editors, *Salt, Shale and Igneous Diapirs in and around Europe* Geological Society, London, Special Publications 174, 1–19
- Vigneresse, J.L., Barbey, P. and Cuney, M. (1996).** Rheological transitions during partial melting and crystallization with application to felsic magma segregation and transfer. *Journal of Petrology.* 37, 1579–1600.
- Westraat, J.D., Kisters, A.F.M., Poujol, M. and Stevens, M. (2005).** Transcurrent shearing, granite sheeting and the incremental construction of the tabular 3.1 Ga Mpuluzi batholith,

Barberton granite–greenstone terrane, South Africa. *Journal of the Geological Society* 162, 373-388.

Yoshinobu, A.S., Okaya, D.A. and Paterson, S.R., (1998). Modelling the thermal evolution of fault-controlled magma emplacement models: implications for the solidification of granitoid plutons. *Journal of Structural Geology* 20, 1205-1218.